The Hubble Constant

Wendy L. Freedman and Barry F. Madore

Carnegie Observatories, Pasadena, California 91101; email: wendy@obs.carnegiescience.edu, barry@obs.carnegiescience.edu

Annu. Rev. Astron. Astrophys. 2010. 48:673–710

First published online as a Review in Advance on June 2, 2010

The *Annual Review of Astronomy and Astrophysics* is online at astro.annualreviews.org

This article's doi:
10.1146/annurev-astro-082708-101829

0066-4146/10/0922-0673$20.00

Key Words

age of Universe, Cepheids, cosmology, distance scale, supernovae

Abstract

Considerable progress has been made in determining the Hubble constant over the past two decades. We discuss the cosmological context and importance of an accurate measurement of the Hubble constant, focusing on six high-precision distance-determination methods: Cepheids, tip of the red giant branch, maser galaxies, surface brightness fluctuations, the Tully-Fisher relation, and Type Ia supernovae. We discuss in detail known systematic errors in the measurement of galaxy distances and how to minimize them. Our best current estimate of the Hubble constant is 73 ± 2 (random) $\pm$ 4 (systematic) km s^{-1} Mpc^{-1}. The importance of improved accuracy in the Hubble constant will increase over the next decade with new missions and experiments designed to increase the precision in other cosmological parameters. We outline the steps that will be required to deliver a value of the Hubble constant to 2% systematic uncertainty and discuss the constraints on other cosmological parameters that will then be possible with such accuracy.

1. INTRODUCTION

In 1929, Carnegie astronomer Edwin Hubble published a linear correlation between the apparent distances to galaxies and their recessional velocities. This simple plot provided evidence that our Universe is in a state of expansion, a discovery that still stands as one of the most profound of the twentieth century (Hubble 1929a). This result had been anticipated earlier by Lemaître (1927), who first provided a mathematical solution for an expanding universe and noted that it provided a natural explanation for the observed receding velocities of galaxies. These results were published in the Annals of the Scientific Society of Brussels (in French) and were not widely known.

Using photographic data obtained at the 100-in Hooker telescope situated at Mount Wilson, California, Hubble measured the distances to six galaxies in the Local Group using the period-luminosity relation (hereafter, the Leavitt Law) for Cepheid variables. He then extended the sample to an additional 18 galaxies reaching as far as the Virgo cluster, assuming a constant upper limit to the brightest blue stars (HII regions) in these galaxies. Combining these distances with published radial velocity measurements (corrected for solar motion), Hubble constructed **Figure 1**. The slope of the velocity versus distance relation yields the Hubble constant, which parameterizes the current expansion rate of the Universe.

The Hubble constant is usually expressed in units of kilometers per second per megaparsec and sets the cosmic distance scale for the present Universe. The inverse of the Hubble constant has dimensions of time. Locally, the Hubble law relates the distance to an object and its redshift: $cz = H_o d$, where d is the distance to the object and z is its redshift. The Hubble law relating the distance and the redshift holds in any Friedman-Lemaître-Robertson-Walker (FLRW) cosmology (see Section 2) for redshifts less than unity. At greater redshifts, the distance-redshift relationship for such a cosmology also depends on the energy densities of matter and dark energy. The exact relation between the expansion age and the Hubble constant depends on the nature of the mass-energy content of the Universe, as discussed further in Sections 2 and 6. In a uniformly expanding universe, the Hubble parameter, $H(t)$, changes as a function of time; H_o, referred to as the Hubble constant, is the value at the current time, t_o.

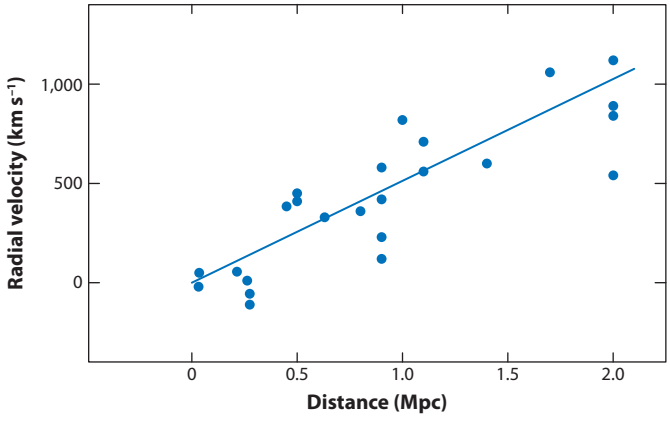

Figure 1

Radial velocities, corrected for solar motion, plotted versus distances estimated from stars and mean luminosities of galaxies in clusters. The solid dots and line represent the solution for solar motion using individual galaxies. Hubble wrote, "The outstanding feature, however, is the possibility that the velocity-distance relation may represent the de Sitter effect, and hence that numerical data may be introduced into discussions of the general curvature of space." (Adapted from Hubble 1929a.)

Measurement of the Hubble constant has been an active subject since Hubble's original measurements of the distances to galaxies: The deceptively simple correlation between galaxy distance and recession velocity discovered 80 years ago did not foreshadow how much of a challenge large systematic uncertainties would pose in obtaining an accurate value for the Hubble constant. Only recently have improvements in linear solid-state detectors, the launch of the *Hubble Space Telescope* (HST), and the development of several different methods for measuring distances led to a convergence on its current value.

Determining an accurate value for H_o was one of the primary motivations for building HST. In the early 1980's, the first director of the Space Telescope Science Institute, Riccardo Giacconi, convened a series of panels to propose observational programs of significant impact requiring large amounts of *Hubble* observations. He was concerned that in the course of any regular time allocation process there would be reluctance to set aside sufficient time to complete such large projects in a timely manner. For decades, a "factor-of-two" controversy persisted, with values of the Hubble constant falling between 50 and 100 km s^{-1} Mpc^{-1}. A goal of 10% accuracy for H_o was designated as one of HST's three "Key Projects." (The other two were a study of the intergalactic medium using quasar absorption lines and a "medium-deep" survey of galaxies.)

This review is organized as follows: We first give a brief overview of the cosmological context for measurements of the Hubble constant. We discuss in some detail methods for measuring distances to galaxies, specifically Cepheids, the tip of the red giant branch (TRGB), masers, surface brightness fluctuations (SBFs), the Tully-Fisher (TF) relation, and Type Ia supernovae (SNe Ia). We then turn to a discussion of H_o, its systematic uncertainties, other methods for measuring H_o, and future measurements of the Hubble constant. Our goal is to describe the recent developments that have resulted in a convergence to better-than-10% accuracy in measurements of the Hubble constant and to outline how future data can improve this accuracy. For wide-ranging previous reviews of this subject, readers are referred to those of Hodge (1982), Huchra (1992), Jacoby et al. (1992), van den Bergh (1992), Jackson (2007), and Tammann, Sandage & Reindl (2008). An extensive monograph by Rowan-Robinson (1985) details the history of the subject as it stood twenty-five years ago.

2. EXPANSION OF THE UNIVERSE: THE COSMOLOGICAL CONTEXT

Excellent introductions to the subject of cosmology can be found in Kolb & Turner (1990) and Dodelson (2003). We give a brief description here to provide the basis for the nomenclature used throughout this review. The expansion of a homogeneous and isotropic universe can be described by an FLRW cosmology, which is characterized by parameters that describe the expansion, the global geometry, and the general composition of the universe. These parameters are all related via the Friedmann equation, derived from the Einstein general relativity field equations:

$$H^2(t) = \left(\frac{\dot{a}}{a}\right)^2 = \frac{8\pi \mathrm{G}}{3} \sum_i \rho_i(t) - \frac{k}{a^2}, \quad (1)$$

where $H(t)$ is the expansion rate, G is the Newtonian gravitational constant, $a(t)$ is the cosmic scale factor characterizing the relative size of the universe at time t to the present scale, $\rho_i(t)$ are the individual components of the matter-energy density, and k (with values of $+1$, 0, or -1) describes the global geometry of the universe. The density ρ_i characterizes the matter-energy composition of the universe: the sum of the densities of baryons, cold dark matter, and hot dark matter; and the contribution from dark energy. Dividing by H^2, we may rewrite the Friedmann equation as $\Omega_{total} - 1 = \Omega_k = k/(a^2 H^2)$. For the case of a spatially flat universe, $k = 0$ and $\Omega_{total} = 1$.

In a matter-dominated universe, the expansion velocity of the Universe slows down over time owing to the attractive force of gravity. However, a decade ago two independent groups

(Perlmutter et al. 1999, Riess et al. 1998) found that supernovae at $z \sim 0.5$ appear to be about 10% fainter than those observed locally, consistent instead with models in which the expansion velocity is increasing; that is, a universe that is accelerating in its expansion. Combined with independent estimates of the matter density, these results are consistent with a universe in which one-third of the overall density is in the form of matter (ordinary plus dark), and two-thirds is in a form having a large, negative pressure, termed dark energy. In this current standard model, the expansion rate of the Universe is given by

$$H^2(z)/H_o^2 = \Omega_{matter}(1+z)^3 + \Omega_{DE}(1+z)^{3(1+w)}, \tag{2}$$

where Ω_{matter} and Ω_{DE} refer to the densities of (ordinary, cold, and hot dark) matter and dark energy, respectively, and $w = p/\rho$ is the equation of state of the dark energy, the ratio of pressure to energy density. Recent observations by the *Wilkinson Microwave Anisotropy Probe* (WMAP), based on entirely independent physics, give results consistent with the supernova data (Komatsu et al. 2009, Dunkley et al. 2009). Under the assumption of a flat universe, the current observations of distant supernovae and measurements by the WMAP satellite are consistent with a cosmological model where $\Omega_{matter} = 0.3$, $\Omega_{vacuum} = 0.7$, and $w = -1$. The observations are inconsistent with cosmological models without acceleration.

Another critical equation from general relativity involving the second derivative of the scale factor is

$$\ddot{a}/a = -4\pi\, G \sum_i (\rho_i + 3\, p_i), \tag{3}$$

where the sum is over the different contributions to the mass-energy density of the Universe. According to this equation, both energy and pressure govern the dynamics of the Universe, unlike the case of Newtonian gravity, where there is no pressure term. It also allows the possibility of negative pressure, resulting in an effective repulsive gravity, consistent with the observations of the acceleration.

Any component of the mass-energy density can be parameterized by its ratio of pressure to energy density, w. For ordinary matter, $w = 0$; for radiation, $w = 1/3$; and for the cosmological constant $w = -1$. The effect on $\ddot{a}/a$ of an individual component is $-4\pi G\rho_i(1+3w_i)$. If $w < -1/3$, then that component will drive an acceleration (positive $\ddot{a}$) of the Universe. The time evolution of the equation of state is unknown; a convenient, simple parameterization is $w(a) = w_o + (1-a)w_a$, where w_o characterizes the current value of w and w_a its derivative.

3. MEASUREMENT OF DISTANCES

In making measurements of extragalactic distances, objects are being observed at a time when the scale factor of the Universe, a, was smaller, and the age of the Universe, t, was younger than at present. Measuring the cosmic expansion generally involves use of one of two types of cosmological distances: the luminosity distance,

$$d_{\rm L} = \sqrt{\frac{L}{4\pi F}}, \tag{4}$$

which relates the observed flux (integrated over all frequencies), F, of an object to its intrinsic luminosity, L, emitted in its rest frame; and the angular diameter distance,

$$d_{\rm A} = \frac{D}{\theta}, \tag{5}$$

which relates the apparent angular size of an object in radians, θ, to its proper size, D. The luminosity and angular diameter distances are related by

$$d_{\rm L} = (1+z)^2 d_{\rm A}. \tag{6}$$

The distance modulus, μ, is related to the luminosity distance as follows:

$$\mu \equiv m - M = 5 \log d_{\rm L} - 5, \tag{7}$$

where m and M are the apparent and absolute magnitudes of the objects, respectively, and $d_{\rm L}$ is in units of parsecs.

The requirements for measuring an accurate value of H_o are simple to list in principle, but are extremely difficult to meet in practice. The measurement of radial velocities from the displacement of spectral lines is straightforward; the challenge is to measure accurate distances. Distance measurements must be obtained far enough away to probe the smooth Hubble expansion (that is, where the random velocities induced by gravitational interactions with neighboring galaxies are small relative to the Hubble velocity), and nearby enough to calibrate the absolute, not simply the relative, distance scale. The objects under study also need to be sufficiently abundant that their statistical uncertainties do not dominate the error budget. Ideally the method has a solid physical underpinning and is established to have high internal accuracy, amenable to empirical tests for systematic errors.

We discuss in detail here three high-precision methods for measuring distances to nearby galaxies: Cepheids, the TRGB method, and maser galaxies. For more distant galaxies, we additionally discuss three methods in detail: the TF relation for spiral galaxies, the SBF method, and the maximum luminosities of Type Ia supernovae (SNe Ia). Although maser distances have so far only been published for two galaxies (NGC 4258 and UGC 3789), this method has considerable potential, perhaps even at distances that probe the Hubble flow directly.

Over the preceding decades, a large number of other "distance indicators" have been explored and applied with varying degrees of success, often over relatively restricted ranges of distance. Main sequence fitting, red giant "clump" stars, RR Lyrae stars, the level of the horizontal branch, Mira variables, novae and planetary nebula luminosity functions (PNLFs), SBFs, globular cluster luminosity functions (GCLFs), as well as red and blue supergiant stars all fall into this class. Some, like the RR Lyrae stars, have provided crucial tests for consistency of zero points but cannot themselves reach very far beyond the Local Group because of their relatively faint intrinsic luminosities. The reader is referred to recent papers on the SN II distance scale (Dessart & Hiller 2005), PNLF (Ciardullo et al. 2002), and fundamental plane (FP) (Blakeslee et al. 2002) and references therein.

Our goal here is not to provide an exhaustive review of all distance determination methods, but rather to focus on a few methods with demonstrably low dispersion, with some currently understood physical basis, and with sufficient overlap with other methods to test quantitatively the accuracy of the calibration and level of systematic errors for the determination of H_o. Before turning to a discussion of methods for measuring distances, we discuss the general issue of interstellar extinction.

3.0.1. Interstellar Extinction. Interstellar extinction systematically decreases a star or galaxy's apparent luminosity. Thus, if extinction is not corrected for, it will result in a derivation of distance that is systematically too large. Dust may be present along the line of sight either within our Milky Way galaxy and/or along the same extended line of sight within the galaxy under study.

Two main observational paths to correct for interstellar extinction have been pursued: (*a*) make observations in at least two wavelength bands and, using the fact that extinction is a known function of wavelength, solve explicitly for the distance and color-excess/extinction effects, or (*b*) observe at the longest wavelengths practical so as to minimize implicitly the extinction effects. The former assumes prior knowledge of the interstellar extinction law and carries the implicit assumption that the extinction law is universal. The latter path is conceptually more robust, given that it simply makes use of the (empirically established) fact that extinction decreases with increasing wavelength. However, working at longer and longer wavelengths has been technically more challenging, so this path has taken longer in coming to fruition.

From studies of Galactic O and B stars, it is well established that interstellar extinction is wavelength-dependent, and from the optical to mid-IR wavelengths it is a generally decreasing function of increasing wavelength (see Cardelli, Clayton & Mathis 1989, Draine 2003 and references therein for empirical and theoretical considerations). Limited studies of stars in external galaxies [primarily the Large Magellanic Cloud (LMC) and the Small Magellanic Cloud (SMC)] support this view, with major departures being confined to the UV region of the spectrum (particularly near 2200 Å). Both for practical reasons (that is, detector sensitivity) and because of the nature of interstellar extinction, the majority of distance-scale applications have avoided the UV, so the most blatant changes in the interstellar extinction curve have been of little practical concern. At another extreme, the universality of the longer-wavelength (optical through IR) portion of the extinction curve appears to break down in regions of intense star formation and extremely high optical depths within the Milky Way. However, the general (diffuse) interstellar extinction curve, as parameterized by ratios of total-to-selective absorption, such as $R_V = A_V / E(B - V)$, appears to be much more stable from region to region. Fortunately Cepheids, TRGB stars, and supernovae are generally not found deeply embedded in very high optical-depth dust but are sufficiently displaced from their original sites of star formation that they are dimmed mostly by the general, diffuse interstellar extinction.

3.1. Cepheid Distance Scale

Since the discovery of the Leavitt Law (Leavitt 1908, Leavitt & Pickering 1912) and its use by Hubble to measure the distances to the Local Group galaxies, NGC 6822 (Hubble 1925), M33 (Hubble 1926), and M31 (Hubble 1929b), Cepheid variables have remained a widely applicable and powerful method for measuring distances to nearby galaxies. In 2009, the American Astronomical Society Council passed a resolution recognizing the 100th anniversary of Henrietta Leavitt's first presentation of the Cepheid period-luminosity relation (Leavitt 1908). The Council noted that it was pleased to learn of a resolution adopted by the organizers of the Leavitt symposium, held in November 2008 at the Harvard-Smithsonian Center for Astrophysics. There, it was suggested that the Cepheid period-luminosity relation should be referred to as the Leavitt Law in recognition of Leavitt's fundamental discovery, and we do so here.

Cepheids are observed to pulsate with periods ranging from 2 to over 100 days, and their intrinsic brightnesses correlate with those periods, ranging from $-2 < M_V < -6$ mag. The ease of discovery and identification of these bright, variable supergiants make them powerful distance indicators. Detailed reviews of the Cepheid distance scale and its calibration can be found in Madore & Freedman (1991), Sandage & Tammann (2006), Fouque et al. (2007), and Barnes (2010). A review of the history of the subject is given by Fernie (1969).

There are many steps that must be taken in applying Cepheids to the extragalactic distance scale. The Cepheids must be identified against the background of fainter, resolved, and unresolved stars that contribute to the surrounding light of the host galaxy. Overcoming crowding and confusion

is the key to the successful discovery, measurement, and use of Cepheids in galaxies beyond the Local Group. From the ground, atmospheric turbulence degrades the image resolution, decreasing the contrast of point sources against the background. In space, the resolution limit is set by the aperture of the telescope and the operating wavelengths of the detectors. HST gives a factor of ten increased resolution over most ground-based telescopes of comparable and larger aperture.

As higher precision data have been accumulated for Cepheids in greater numbers and in different physical environments, it has become possible to search for and investigate a variety of lower level, but increasingly important, systematics affecting the Leavitt Law. Below we briefly discuss these complicating effects (reddening and metallicity, specifically) and their uncertainties, and quantify their impact on the extragalactic distance scale. We then elaborate on methods for correcting for and/or mitigating their impact on distance determinations. But first we give an overview of the physical basis for the Leavitt Law in general terms.

3.1.1. Underlying Physics. The basic physics connecting the luminosity and color of a Cepheid to its period is well understood. Using the Stephan-Boltzmann law,

$$L = 4\pi R^2 \sigma T_e^4, \tag{8}$$

the bolometric luminosities, L, of all stars, including Cepheids, can be derived. Expressed in magnitudes, the Stefan-Boltzmann Law becomes

$$M_{BOL} = -5 \log R - 10 \log T_e + C. \tag{9}$$

Hydrostatic equilibrium can be achieved for long periods of time along the core helium-burning main sequence. As a result, stars are constrained to reside there most of the time, thereby bounding the permitted values of the independent radius and temperature variables for stars in the $M_{BOL} - \log T_e$ plane.

If $\log T_e$ is mapped into an observable intrinsic color [that is, $(B-V)_o$] and radius is mapped into an observable period (through a period-mean-density relation), the period-luminosity-color (PLC) relation for Cepheids can be determined (e.g., Sandage 1958, Sandage & Gratton 1963, Sandage & Tammann 1968). In its linearized form for pulsating variables, the Stefan-Boltzmann law takes on the following form of the PLC: $M_V = \alpha \log P + \beta(B-V)_o + \gamma$.

Cepheid pulsation occurs because of the changing atmospheric opacity with temperature in the helium ionization zone. This zone acts like a heat engine and valve mechanism. During the portion of the cycle when the ionization layer is opaque to radiation, that layer traps energy, resulting in an increase in its internal pressure. This added pressure acts to elevate the layers of gas above it, resulting in the observed radial expansion. As the star expands, it does work against gravity and the gas cools. As it does so, its temperature falls back to a point where the doubly ionized helium layer recombines and becomes transparent again, thereby allowing more radiation to pass. Without that added source of heating the local pressure drops, the expansion stops, the star recollapses, and the cycle repeats. The alternate trapping and releasing of energy in the helium ionization layer ultimately gives rise to the periodic change in radius, temperature, and luminosity seen at the surface. Not all stars are unstable to this mechanism. The cool (red) edge of the Cepheid instability strip is thought to be controlled by the onset of convection, which then prevents the helium ionization zone from driving the pulsation. For hotter temperatures, the helium ionization zone is located too far out in the atmosphere for significant pulsations to occur. Further details can be found in the classic stellar pulsation textbook by Cox (1980).

Cepheids have been intensively modeled numerically, with increasingly sophisticated hydrodynamical codes (for a recent review, see Buchler 2010). Although continuing progress is being made, the challenges remain formidable in following a dynamical atmosphere and in modeling

convection with a time-dependent mixing length approximation. In general, observational and theoretical PLC relations are in reasonable agreement (e.g., Caputo 2008). However, as discussed in Section 3.1.3, subtle effects (for example, the effect of metallicity on Cepheid luminosities and colors) remain difficult to predict from first principles.

3.1.2. Cepheids and Interstellar Extinction. If one adopts a mean extinction law and applies it universally to all Cepheids, regardless of their parent galaxy's metallicity, then one can use the observed colors and magnitudes of the Cepheids to correct for the total line-of-sight extinction. If, for example, observations are made at V and I wavelengths (as is commonly done with HST), and the ratio of total-to-selective absorption $R_{VI} = A_V/E(V-I)$ is adopted a priori (e.g., Cardelli, Clayton & Mathis 1989), then one can form from the observed colors and magnitudes an extinction-free, Wesenheit magnitude, W, (Madore 1982), defined by

$$W = V - R_{VI} \times (V - I), \tag{10}$$

as well as an intrinsic Wesenheit magnitude, W_o:

$$W_o = V_o - R_{VI} \times (V - I)_o. \tag{11}$$

By construction,

$$W = V_o + A_V - R_{VI} \times (V - I)_o - R_{VI} \times E(V - I) \tag{12}$$

$$= V_o - R_{VI}(V - I)_o + A_V - R_{VI} \times E(V - I), \tag{13}$$

where $V = V_o + A_V$ and $(V - I) = (V - I)_o + E(V - I)$, and $A_V = R_{VI} \times E(V - I)$, thereby reducing the last two terms to zero, leaving $W = V_o - R_{VI} \times (V - I)_o$, which is equivalent to the definition of W_o.

The numerical value of W as constructed from observed data points is numerically identical to the intrinsic (unreddened) value of the Wesenheit function, W_o. Thus, W, for any given star, is dimmed only by distance and (by its definition) it is unaffected by extinction, again only to the degree that R is known and is universal. W can be formed for any combination of optical/near-IR bandpasses.

3.1.3. Metallicity. The atmospheres of stars like Cepheids, having effective temperatures typical of G and K supergiants, are affected by changes in the atmospheric metal abundance. There are additionally changes in the overall stellar structure (the mass-radius relation) due to changes in chemical composition. Thus, it is expected that the colors and magnitudes of Cepheids, and their corresponding period-luminosity (PL) relations, should be a function of metallicity. However, predicting the magnitude (and even simply the sign of the effect) at either optical or even longer wavelengths, has proven to be challenging: Different theoretical studies have led to a range of conclusions. We review below the empirical evidence. For a comparison with recent theoretical studies, we refer the interested readers to papers by Sandage, Bell & Tripicco (1999), Bono et al. (2008), Caputo (2008), and Romaniello et al. (2008, 2009).

Two tests of the metallicity sensitivity of the Leavitt Law have been proposed. The first test uses measured radial metallicity gradients within individual galaxies to provide a differential test in which observed changes in the Cepheid zero point with radius are ascribed to changes in metallicity. This test assumes that the Cepheids and the HII regions (which calibrate the measured [O/H] abundances) share the same metallicity at a given radius and that other factors are not contributing to a zero-point shift, such as radially dependent crowding or changes of the extinction law with radius, etc. The second test uses the difference between Cepheid and TRGB distances for galaxies

with both measurements and seeks a correlation of these differences as a function of the Cepheid (that is, HII region) metallicity.

The first test, leveraging metallicity gradients in individual galaxies, has been undertaken for M31 (Freedman & Madore 1990), M101 (Kennicutt et al. 1998), NGC 4258 (Macri et al. 2006), and M33 (Scowcroft et al. 2009). The second test, comparing TRGB and Cepheid distances, was first made by Lee, Freedman & Madore (1993). Udalski et al. (2001) used a newly observed sample of Cepheids in IC 1613 in comparison to a TRGB distance to that same galaxy and concluded that, in comparison with the SMC, LMC, and NGC 6822, there was no metallicity effect over a factor of two in metallicity at low mean metallicity. An extensive cross comparison of Cepheid and TRGB distances including high-metallicity systems is well summarized by Sakai et al. (2004). Individual datasets and metallicity calibrations are still being debated, but the general concensus is that for the reddening-free W(VI) calibration of the Cepheid distance scale there is a metallicity dependence that, once corrected for, increases the distance moduli of higher metallicity Cepheids if their distances are first determined using a lower metallicity (e.g., LMC) PL calibration. However, in a different approach, Romaniello et al. (2008) obtained direct spectroscopic [Fe/H] abundances for a sample of Galactic, LMC, and SMC Cepheids. They compare the Leavitt Law for samples of stars with different mean metallicities and, in contrast, they find an increasing dependence of the V-band residuals with [Fe/H] abundance that is in the opposite sense to these previous determinations. Clearly, the effect of metallicity on the observed properties of Cepheids is still an active and on-going area of research.

A remaining uncertainty at the end of the H_o Key Project (described further in Section 4) was due to the fact that the majority of Key Project galaxies have metallicities more comparable to the Milky Way than to the LMC, which was used for the calibration. Below, in Section 3.1.4, we ameliorate this systematic error by adopting a Galactic calibration provided by new trigonometric parallaxes of Milky Way Cepheids not available at the time of the Key Project. By renormalizing to a high-metallicity (Galactic) calibration for the Cepheids, metallicity effects are no longer a major systematic, but rather a random error, whose size will decrease with time as the sample size increases. Based on the Cepheid metallicity calibration of Sakai et al. (2004) (with adopted LMC and solar values for 12 + log (O/H) of 8.50 and 8.70, respectively; and a metallicity slope of 0.25 mag dex^{-1}), we estimate the metallicity correction in transforming from an LMC to a Galactic-based Cepheid zero point to be $0.25 \times 0.2 = 0.05$ mag, with a residual scatter of about ± 0.07 mag.

3.1.4. Galactic Cepheids with Trigonometic Parallaxes. An accurate trigonometric parallax calibration for Galactic Cepheids has been long sought, but very difficult to achieve in practice. All known classical (Galactic) Cepheids are more than 250 pc away: Therefore, for direct distance estimates good to 10%, parallax accuracies of ± 0.2 marcsec are required, necessitating space observations. The *High Precision Parallax Collecting Satellite* (Hipparchos) reported parallaxes for 200 of the nearest Cepheids, but (with the exception of Polaris) even the best of these were of very low signal-to-noise ratios (Feast & Catchpole 1997).

Recent progress has come with the use of the Fine Guidance Sensor on HST (Benedict et al. 2007), whereby parallaxes, in many cases accurate to better than $\pm 10\%$ for individual stars, were obtained for 10 Cepheids spanning the period range 3.7 to 35.6 days. We list the distance moduli, errors, and distances for these Cepheids in **Table 1**. These nearby Cepheids span a range of distances from about 300 to 560 pc.

The calibration of the Leavitt relation based on these ten stars leads to an error on their mean of $\pm 3\%$ (or ± 0.06 mag), which we adopt here as the systematic error on the distance to the LMC discussed below, and the Cepheid zero point, in general. In what follows, we adopt the

Table 1 Galactic cepheids with geometric parallaxes

Cepheid	P(days)	log P	μ (mag)	σ (%)	Distance (pc)
RT Aur	3.728	0.572	8.15	7.9	427
T Vul	4.435	0.647	8.73	12.1	557
FF Aql	4.471	0.650	7.79	6.4	361
δ Cep	5.366	0.730	7.19	4.0	274
Y Sgr	5.773	0.761	8.51	13.6	504
X Sgr	7.013	0.846	7.64	6.0	337
W Sgr	7.595	0.881	8.31	8.8	459
β Dor	9.842	0.993	7.50	5.1	316
ζ Gem	10.151	1.007	7.81	6.5	365
ℓ Car	35.551	1.551	8.56	9.9	515

zero point based on the Galactic calibration, but retain the slope based on the LMC, because the sample size is still much larger and statistically better defined. Improvement of this calibration (both slope and zero point) awaits a larger sample of (long-period) Cepheids from the *Global Astrometric Interferometer for Astrophysics* (GAIA). We have adopted a zero-point calibration based both on these HST data, as well as a calibration based on the maser galaxy, NGC 4258 (Section 3.3), and present a revised value of H_o in Section 4.

A significant systematic at this time is the Galactic calibration zero point. Its value depends on only ten stars, each of which have individual uncertainties in their distances that are each at the 10% level. Given the small sample size of the Galactic calibrators, the error on their mean can be no better than 3% (or ± 0.06 mag), which we adopt here as the newly revised systematic error on the distance to the LMC, and the Cepheid zero point in general. In what follows, we adopt the zero point based on the Galactic calibration, but retain the slope based on the LMC, because the sample size is still much larger and statistically better defined. There has recently been discussion in the literature about possible variations in the slope of the Leavitt Law occurring around 10 days (see Ngeow, Kanbur & Nanthakumar (2008) and references therein); however, Riess et al. (2009b) and Madore & Freedman (2009) both find that when using W, the differences are not statistically significant. Improvement of this calibration (both slope and zero point) awaits a larger sample of (long-period) Cepheids from GAIA.

3.1.5. The Distance to the Large Magellanic Cloud. Because of the abundance of known Cepheids in the LMC, this galaxy has historically played a central role in the calibration of the Cepheid extragalactic distance scale. Several thousand Cepheids have been identified and cataloged in the LMC (Leavitt 1908, Alcock et al. 2000, Soszynski et al. 2008), all at essentially the same distance. Specifically, the slope of the Leavitt Law is both statistically and systematically better determined in the LMC than it is for Cepheids in our own Galaxy. This is especially true for the long-period end of the calibration where the extragalactic samples in general are far better populated than the more restricted Milky Way subset available in close proximity to the Sun. In **Figure 2**, we show the range of values of LMC distance moduli based on non-Cepheid moduli, published up to 2008. The median value of the non-Cepheid distance moduli is 18.44 ± 0.16 mag.

Based on the new results for direct geometric parallaxes to Galactic Cepheids (Benedict et al. 2007) discussed in Section 3.1.4, we calibrate the sample of LMC Cepheids used as fiducial for the HST Key Project. The new Galactic parallaxes now allow a zero point to be obtained for the Leavitt Law. In **Figure 3**, we show BVIJHK Leavitt Laws for the Galaxy and LMC calibrated

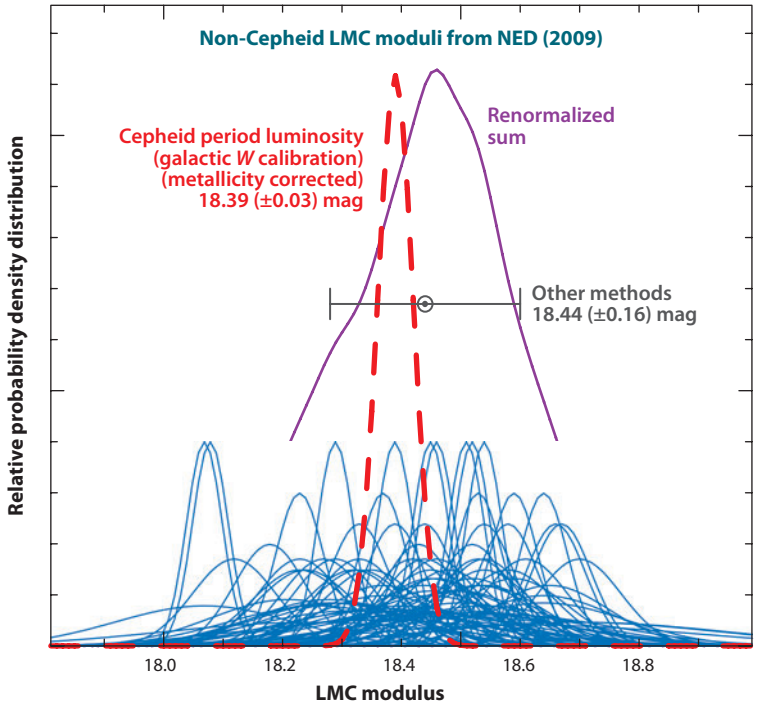

Figure 2

The cumulative probability density distribution of 180 distance modulus estimates to the Large Magellanic Cloud (LMC) culled from the recent literature and provided by the NASA/IPAC Extragalactic Database (NED). Individual estimates are shown by unit-area Gaussians with a dispersion set to their quoted statistical errors (*thick blue lines)*. The thin solid purple line represents the renormalized sum of those Gaussians. The thick broken red line represents the value of 18.39 mag and a systematic error of ± 0.03 mag for the true (Wesenheit, *W*) distance modulus to the LMC, based on the Galactic parallax calibration for Cepheids and corrected for metallicity by -0.05 mag. For comparison, the median value of the published, non-Cepheid distance moduli is 18.44 ± 0.16 mag (shown as the *circled gray point and error bar*); the mode of the non-Cepheid moduli is 18.47 mag. The Cepheid value is statistically indistinguishable from this highly heterogeneous, but fairly complete, set of independently published determinations.

with the new parallaxes. As can be seen, the slope of the Leavitt Law increases with increasing wavelength, with a corresponding decrease in dispersion. In the past, because of the uncertainty in the Galactic Cepheid calibration, a distance modulus to the LMC and the mean Cepheid extinction were obtained using a combination of several independent methods. Multiwavelength Leavitt Laws were then used to obtain differential extragalactic distances and reddenings for galaxies beyond the LMC. We can show here for the first time the multiwavelength solution for the distance to the LMC itself based on the apparent BVIJHK Cepheid distance moduli, fit to a Cardelli, Clayton & Mathis (1989) extinction curve, and adopting a Galactic calibration for the zero point and the slope from the LMC data. The LMC apparent moduli, scaled to the Galactic calibration, are shown as a function of inverse wavelength in **Figure 4**. The data are well fit by a Galactic extinction law having a scale factor corresponding to $E(\mathrm{B}-\mathrm{V}) = 0.10$ mag and an intercept at $1/\lambda = 0.00$, corresponding to a true modulus of $\mu(\mathrm{LMC})_o = 18.40 \pm 0.01$ mag.

The composite (Galactic + LMC) VI Wesenheit function is shown in **Figure 5**. The correspondence between the two independent Cepheid samples is good, and the dispersion in *W* remains

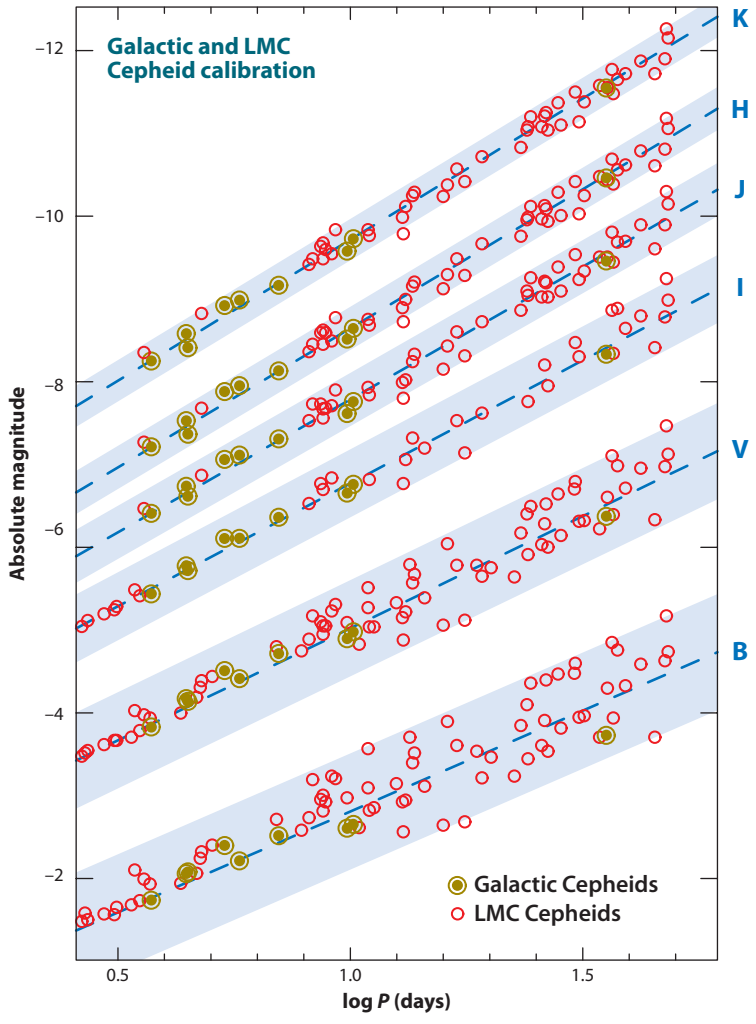

Figure 3

Composite multiwavelength period-luminosity (PL) relations (Leavitt Laws) for Galactic (*circled filled dark yellow dots*) and Large Magellanic Cloud (LMC) (*open red circles*) Cepheids from the optical (BVI) through the near-IR (JHK). There is a monotonic increase in the slope, coupled with a dramatic decrease in total dispersion of the PL relations as one goes to longer and longer wavelengths.

very small. The Wesenheit function uses fewer wavelengths, but it employs the two bandpasses directly associated with the HST Key Project and most extragalactic Cepheid distances, and so we adopt it here.

The W(V,VI) Wesenheit function gives a minimized fit between the Galactic and the LMC Cepheids corresponding to a true distance modulus of $\mu(\mathrm{LMC})_o = 18.44 \pm 0.03$ mag. Correcting for metallicity (see Section 3.1.3) would decrease this to 18.39 mag. Because of the large numbers of Cepheids involved over numerous wavelengths, the statistical errors on this value are small; and once again, systematic errors dominate the error budget. As discussed in Section 3.1.4, we adopt a newly revised systematic error on the distance to the LMC of 3% (or ± 0.06 mag).

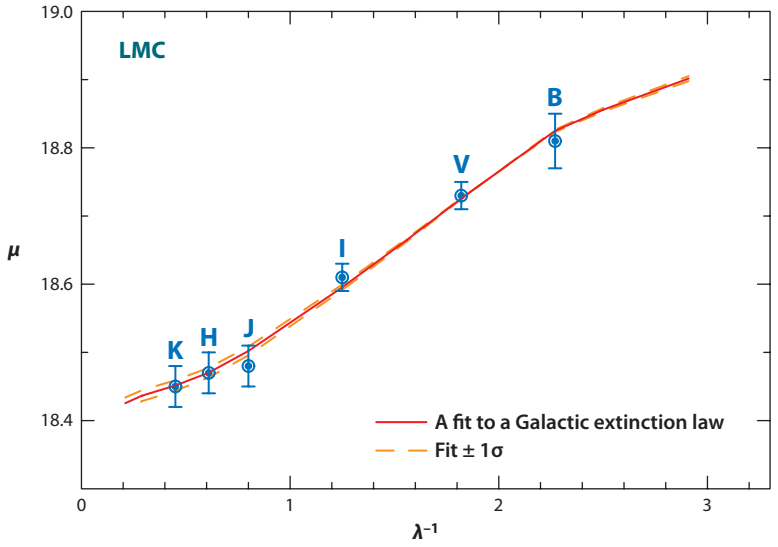

Figure 4

Standard extinction curve fit to six multiwavength (BVIJHK) apparent distance moduli to the Large Magellanic Cloud (LMC) scaled to the *Hubble Space Telescope* Galactic parallax sample (Benedict et al. 2007). The minimized χ^2 scaled fit gives a true distance modulus (intercept) of 18.40 ± 0.01 mag, uncorrected for metallicity, and a total line-of-sight color excess (slope) of $E(B - V) = 0.10$ mag.

As noted above, the main drawback to using the LMC as the fundamental calibrator of the Leavitt Law is the fact that the LMC Cepheids are of lower metallicity than many of the more distant spiral galaxies useful for measuring the Hubble constant. This systematic is largely eliminated by adopting the higher metallicity Galactic calibration as discussed in Section 3.1.3 or the NGC 4258 calibration discussed in Section 3.3.

3.2. Tip of the Red Giant Branch Method

As discussed briefly in Section 3.1.3, a completely independent method for determining distances to nearby galaxies that has comparable precision to Cepheids is TRGB. The TRGB method uses the theoretically well-understood and observationally well-defined discontinuity in the luminosity function of stars evolving up the red giant branch in old, metal-poor stellar populations. This feature has been calibrated using Galactic globular clusters, and because of its simplicity and straightforward application, it has been widely used to determine distances to nearby galaxies. Recent and excellent reviews of the topic are given by Rizzi et al. (2007) and Bellazzini (2008).

Using the brightest stars in globular clusters to estimate distances has a long history [ultimately dating back to Shapley (1930), and later discussed again by Baade (1944)]. The method gained widespread application in a modern context in two papers: one by Da Costa & Armandroff (1990, for Galactic globular clusters) and the other by Lee, Freedman & Madore (1993, where the use of a quantitative digital filter to measure the tip location was first introduced in an extragalactic context).

Approximately 250 galaxies have had their distances measured by the TRGB method, compared to a total of 57 galaxies with Cepheid distances. (A comprehensive compilation of

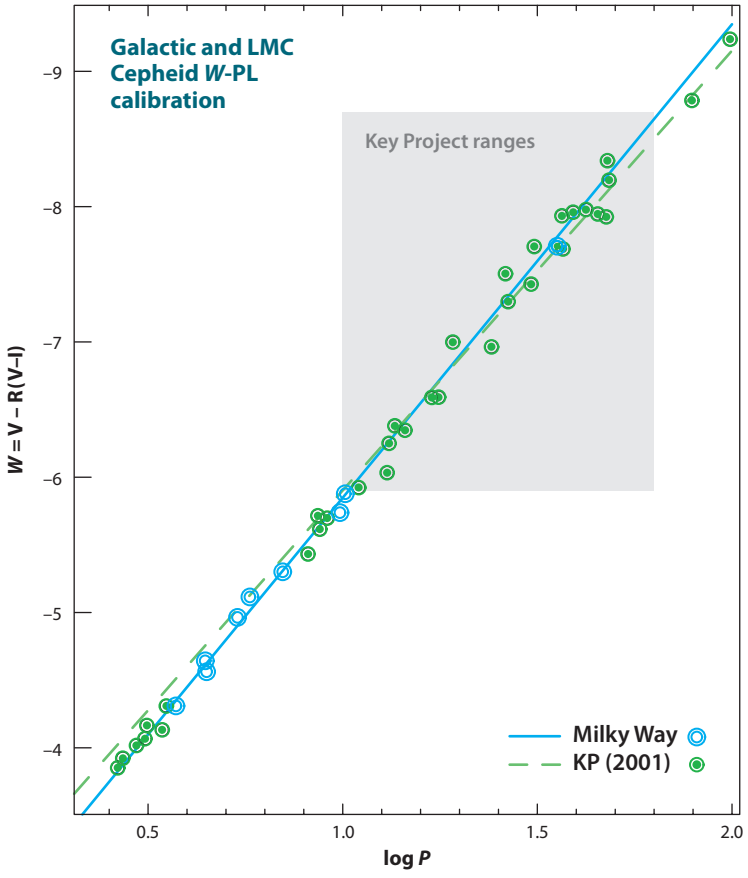

Figure 5

The reddening-free VI Wesenheit period-luminosity (*W*-PL) relation showing the combined data for Galactic Cepheids having individually determined trigonometric parallaxes (*circled green dots*) and Large Magellanic Cloud (LMC) Cepheids (*open blue circles*) brought into coincidence with the Galactic calibration after an offset of 18.44 mag between their apparent magnitudes. The solid blue line is a fit to the combined data. The dashed green line is the calibration used by Freedman et al. (2001) at the conclusion of the Key Project (KP). The gray inner bounding box shows the period and luminosity range used by the Key Project to determine extragalactic distances. The correspondence between the two calibrations is very close, but it should be noted that the Galactic calibration is for Galactic metallicity.

direct distance determinations is available at the following Web site: **http://nedwww.ipac.caltech.edu/level5/NED1D/ned1d.html**). In practice, the TRGB method is observationally a much more efficient technique, because, unlike for Cepheid variables, there is no need to follow them through a variable light cycle: A single-epoch observation, made at two wavelengths (to provide color information) is sufficient. A recent example of applying the TRGB technique to the maser galaxy, NGC 4258, is shown in **Figure 6**.

3.2.1. Theory. The evolution of a post main-sequence, low-mass star up the red giant branch is one of the best-understood phases of stellar evolution (e.g., Iben & Renzini 1983). For the stars of interest in the context of the TRGB, a helium core forms at the center, supported by electron degeneracy pressure. Surrounding the core and providing the entire luminosity of the

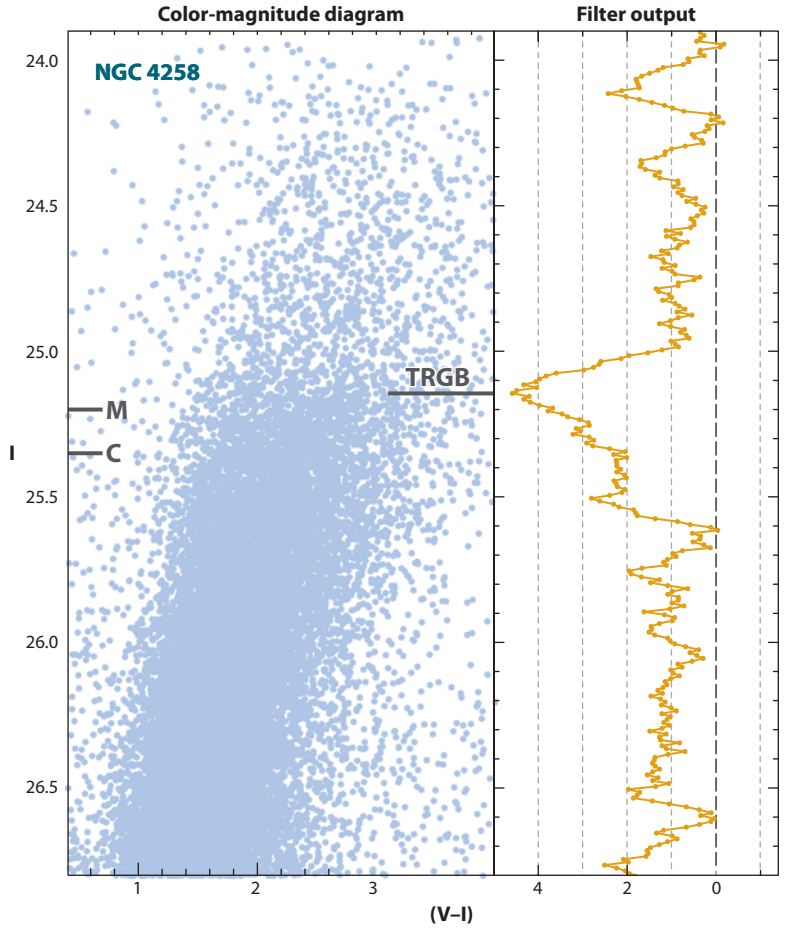

Figure 6

An example of the detection and measurement of the discontinuity in the observed luminosity function for red giant branch stars in the halo of the maser galaxy NGC 4258 (Mager, Madore & Freedman 2008). The color-magnitude diagram on the left has been adjusted for metallicity such that the tip of the red giant branch (TRGB) is found at the same apparent magnitude independent of color/metallicity of the stars at the tip. The right panel shows the output of an edge-detection (modified Sobel) filter (*yellow line*), whose peak response indicates the TRGB magnitude and whose width is used as a measure of the random error on the detection.

star is a hydrogen burning shell. The "helium ash" from the shell increases the mass of the core systematically with time. In analogy with the white dwarf equation of state and the consequent scaling relations that interrelate core mass, M_c, and core radius, R_c, for degenerate electron support, the core (that is, shell) temperature, T_c, and the resulting shell luminosity are simple functions of M_c and R_c alone: $T_c \sim M_c/R_c$ and $L_c \sim M_c^7/R_c^5$. As a result, the core mass increases, the radius simultaneously shrinks, and the luminosity increases due to both effects. The star ascends the red giant branch with increasing luminosity and higher core temperatures. When T_c exceeds a physically well-defined temperature, helium ignites throughout the core. The helium core ignition does not make the star brighter, but rather it eliminates the shell source by explosively heating and thereby lifting the electron degeneracy within the core. This dramatic change in the equation of state is such that the core flash (which generates the equivalent instantaneous luminosity of an

entire galaxy) is internally quenched in a matter of seconds, inflating the core and settling down to a lower luminosity, helium core–burning main sequence. The transition from the red giant to the horizontal branch occurs rapidly (within a few million years) so that observationally the TRGB can be treated as a physical discontinuity. A stellar evolutionary "phase change" marks the TRGB. The underlying power of the TRGB is that it is a physically-based and theoretically well-understood method for determining distance. Nuclear physics fundamentally controls the stellar luminosity at which the RGB is truncated, which is essentially independent of the chemical composition and/or residual mass of the envelope sitting above the core.

The radiation from stars at the TRGB is redistributed with wavelength as a function of the metallicity and mass of the envelope. Empirically it is found that the bolometric corrections are smallest in the *I*-band, and most recent measurements have been made at this wavelength. The small residual metallicity effect on the TRGB luminosity is well documented and can be empirically calibrated out (see Madore, Mager & Freedman 2009).

3.2.2. Recent Tip of the Red Giant Brance Results and Calibration of the Hubble Constant. In the context of measuring the Hubble constant, red giant branch stars are not as bright as Cepheids, and therefore cannot be seen as far, but they can still be seen to significant distances (~20 Mpc and including Virgo; e.g., Durrell et al. 2007, Caldwell 2006), and as we have seen, they can serve an extremely important function as an independent test of the Cepheid distance scale and check on systematic effects.

Mould & Sakai (2008) have used the TRGB as an alternate calibration to the Cepheid distance scale for the determination of H_o. They use 14 galaxies for which TRGB distances can be measured to calibrate the TF relation and determine a value of $H_o = 73 \pm 5$ (statistical only) km s^{-1} Mpc^{-1}, a value about 10% higher than found earlier by Sakai et al. (2000) based on a Cepheid calibration of 23 spiral galaxies with TF measurements. In subsequent papers, they calibrate the SBF method (Mould & Sakai 2009a) and then go on to check the calibration of the FP for early-type galaxies and the luminosity scale of Type Ia supernovae (Mould & Sakai 2009b). They conclude that the TRGB and Cepheid distances scales are all consistent using SBF, FP, SNe Ia, and the TF relation.

3.3. Maser Galaxies

H_2O mega-masers have recently been demonstrated to be a powerful new geometric tool for accurately measuring extragalactic distances. An extensive review of both the physical nature and the application of mega-masers to the extragalactic distance scale can be found in Lo (2005). The technique utilizes the mapping of 22.2 GHz water maser sources in the accretion disks of massive black holes located in spiral galaxies with active galactic nuclei through modeling of a rotating disk ideally in pure Keplerian motion. In the simplest version of the technique, a rotation curve is measured along the major axis of the disk; proper motions are measured on the near side of the disk minor axis, and a comparison of the angular velocities in the latter measurement with the absolute velocities in km s^{-1} in the former measurements yields the distance.

The method requires a sample of accretion disks that are relatively edge on (so that a rotation curve can be obtained from radial-velocity measurements) and a heating source such as X-rays or shocks to produce maser emission. The basic assumption is that the maser emission arises from trace amounts of water vapor ($<10^{-5}$ in number density) in very small density enhancements in the accretion disk and that they act as perfect dynamical test particles. The maser sources appear as discrete peaks in the spectrum or as unresolved spots in the images constructed from Very Long Baseline Interferometry (VLBI). Measurements of the acceleration ($a = V^2/r$) are obtained directly by monitoring the change of maser radial velocities over time from single-dish

observations. Proper motions are obtained from observed changes in angular position in interferometer images. The approximately Keplerian rotation curve for the disk is modeled, allowing for warps and radial structure. The best-studied galaxy, NGC 4258, at a distance of about 7 Mpc, is too close to provide an independent measurement of the Hubble constant (that is, free from local velocity-field perturbations), but it serves as an invaluable independent check of the Cepheid zero-point calibration.

3.3.1. A Maser Distance to NGC 4258. VLBI observations of H_2O maser sources surrounding the active galactic nucleus of NGC 4258 reveal them to be in a very thin, differentially rotating, slightly warped disk. The Keplerian velocity curve has deviations of less than 1%. The disk has a rotational velocity in excess of 1,000 km s^{-1} at distances on the order of 0.1 pc from the inferred supermassive (10^7 $M_\odot$) nuclear black hole. Detailed analyses of the structure of the accretion disk as traced by the masers have been published (e.g., Herrnstein et al. 1999, Humphreys et al. 2008 and references therein). Over time it has been possible to measure both proper motions and accelerations of these sources and thereby allow for the derivation of two independent distance estimates to this galaxy. The excellent agreement of these two estimates supports the a priori adoption of the Keplerian disk model and gives distances of 7.2 ± 0.2 and 7.1 ± 0.2 Mpc, respectively.

Because of the simplicity of the structure of the maser system in NGC 4258 and its relative strength, NGC 4258 will remain a primary test bed for studying systematic effects that may influence distance estimates. Several problems may limit the ultimate accuracy of this technique, however. For example, because the masers are only distributed over a small angular part of the accretion disk, it is difficult to assess the importance of noncircular orbits. Of possible concern, eccentric disks of stars have been observed in a number of galactic nuclei, where the potential is dominated by the black hole, as is the case for NGC 4258. In addition, even if the disk is circular, it is not a given that the masers along the minor axis are at the same radii as the masers along the major axis.

The self-gravity of the disk also may need to be investigated and modeled because the maser distribution suggests the existence of spiral arms (Humphreys et al. 2008). Finally, radiative transfer effects may cause nonphysical motions in the maser images. Although the current agreement of distances using several techniques is comforting, having only one sole calibrating galaxy for this technique remains a concern, and further galaxies will be required to ascertain the limiting uncertainty in this method.

3.3.2. Other Distance Determinations to NGC 4258. The first Cepheid distance to NGC 4258 was published by Maoz et al. (1999), who found a distance of 8.1 ± 0.4 Mpc based on an LMC-calibrated distance modulus of 18.50 mag. Newman et al. (2001) found a distance modulus of 29.47 ± 0.09 (random) $\pm$ 0.15 (systematic), giving a distance of $7.83 \pm 0.3 \pm 0.5$ Mpc. Macri et al. (2006) reobserved NGC 4258 in two radially (and chemically) distinct fields, discovering 281 Cepheids at BV and I wavelengths. Their analysis gives a distance modulus of $29.38 \pm 0.04 \pm 0.05$ mag (7.52 ± 0.16 Mpc), if one adopts μ(LMC) = 18.50 mag. Several more recent determinations of resolved-star (Cepheid and TRGB) distance moduli to NGC 4258 are in remarkably coincident agreement with the maser distance modulus. di Benedetto (2008) measures a Cepheid distance modulus of $29.28 \pm 0.03 \pm 0.03$ for NGC 4258, corresponding to a distance of 7.18 Mpc; Benedict et al. (2007) also find a distance modulus of 29.28 ± 0.08 mag; and Mager, Madore & Freedman (2008) also find a value of $29.28 \pm 0.04 \pm 0.12$ mag both from Cepheids and from the TRGB method. These latter studies are in exact agreement with the current maser distance. Higher accuracy has come from larger samples with higher signal-to-noise data and improved treatment of metallicity.

An alternative approach to utilizing the maser galaxy in the distance scale is to adopt the geometric distance to NGC 4258 as foundational, use it to calibrate the Leavitt Law, and from there determine the distance to the LMC. Macri et al. (2006) adopt this approach and conclude that the true distance modulus to the LMC is 18.41 ± 0.10 mag. This value agrees well with the new Galactic Cepheid calibration of the LMC Leavitt law, as discussed in Section 3.1.5.

3.3.3. NGC 4258 and the Calibration of H_o. The distance to NGC 4258 can be used to leapfrog over the LMC altogether to calibrate the Cepheid PL relation and then secondary methods. Macri et al. (2006) and Riess et al. (2009a,b) have adopted the distance to NGC 4258 as a calibration of the supernova distance scale, as discussed further in Section 3.5.2.

Attempts to measure distances to other megamasers has proven difficult. About 2,000 galaxies have been surveyed for masers, and more than 100 masers have been discovered to date. The detection rate of about 5% is likely due to detection sensitivity and the geometric constraint that the maser disk be viewed nearly edge on because the maser emission is expected to be highly beamed in the plane of the disk. About 30 of these masers have spectral profiles indicative of emission from thin disks, that is, masers at the galactic systemic velocity and groups of masers symmetrically spaced in velocity. About a dozen maser galaxies are sufficiently strong that they can be imaged with phase-referenced VLBI techniques. Only about 5 have been found to have sufficiently simple structure so that they can be fit to dynamical models and have their distances determined. The most promising examples of these galaxies is UGC 3789, which has a recessional velocity of greater than 3,000 km s^{-1} and is being pursued by the Megamaser Cosmology Project (Reid et al. 2009).

If a significant number of maser galaxies can be found and precisely observed well into the Hubble flow, this method can, in principle, compete with methods such as SNe Ia for measuring H_o. The challenge will be to obtain large enough sample sizes of hundreds of objects, in order to average over large-scale flows. Unfortunately, this likely will not be accomplished in the upcoming decade. It is also hoped that nearby objects will be found where this technique can be applied, in addition to NGC 4258, and strengthen the zero-point calibration of the extragalactic distance scale. The future for this technique (beyond 2020) looks promising, given a high-frequency capability for the Square Kilometer Array.

3.4. Surface Brightness Fluctuation (SBF) Method

For distances to elliptical galaxies and early-type spirals with large bulge populations, the SBF method, first introduced by Tonry & Schneider (1988), overlaps with and substantially exceeds the current reach of the TRGB method. Both methods use properties of the red giant branch luminosity function to estimate distances. The SBF method quantifies the effect of distance on an over-all measure of resolution of the Population II red giant stars, naturally weighted both by their intrinsic luminosities and relative numbers. What is measured is the pixel-to-pixel variance in the photon statistics (scaled by the surface brightness) as derived from an image of a pure population of red giant branch stars. For fixed surface brightness, the variance in a pixel (of fixed angular size) is a function of distance, simply because the total number of discrete sources contributing to any given pixel increases with the square of the distance. Although the TRGB method relies entirely on the very brightest red giant stars, the SBF method uses a luminosity-weighted integral over the entire RGB population in order to define a typical "fluctuation star" whose mean magnitude, $\overline{M_I}$, is assumed to be universal and can therefore be used to derive distances. For recent discussions of the SBF method, the reader is referred to Biscardi et al. (2008) and Blakeslee et al. (2009).

Aside from the removal of obvious sources of contamination such as foreground stars, dust patches, and globular clusters, the SBF method does require some additional corrections. It is well known that the slope of the red giant branch in the color-magnitude diagram is a function of metallicity, and so the magnitude of the fluctuation star is both expected and empirically found to be a function of metallicity. A (fairly steep) correction for metallicity has been derived and can be applied using the mean color of the underlying stellar population $\overline{M_I} = -1.74 + 4.5(V - I)_o - 1.15$ (Tonry et al. 2002).

A recent and comprehensive review of the application of the SBF method to determining cosmic distances, and its comparison to the FP method is given in Blakeslee et al. (2002). Over 170 galaxies enter into the comparison; this analysis leads to the conclusion that $H_o = 72 \pm 4$ (random) ± 11 (systematic) km s^{-1} Mpc^{-1}.

3.5. Tully-Fisher Relation

The total luminosity of a spiral galaxy (corrected to face-on inclination to account for extinction) is strongly correlated with the galaxy's maximum (corrected to edge-on inclination) rotation velocity. This relation, calibrated via the Leavitt Law or TRGB, becomes a powerful means of determining extragalactic distances (Tully & Fisher 1977, Aaronson et al. 1986, Pierce & Tully 1988, Giovanelli et al. 1997). The TF relation at present is one of the most widely applied methods for distance measurements, providing distances to thousands of galaxies both in the general field and in groups and clusters. The scatter in this relation is wavelength-dependent and approximately ± 0.3–0.4 mag or 15–20% in distance (Giovanelli et al. 1997, Sakai et al. 2000, Tully & Pierce 2000).

In a general sense, the TF relation can be understood in terms of the virial relation applied to rotationally supported disk galaxies, under the assumption of a constant mass-to-light ratio (Aaronson, Huchra & Mould 1979). However, a detailed self-consistent physical picture that reproduces the TF relation (e.g., Steinmetz & Navarro 1999) and the role of dark matter in producing almost universal spiral galaxy rotation curves (McGaugh et al. 2000) still remains a challenge.

Spitzer Space Telescope archival data have recently yielded an unexpected and exciting discovery. Of the 23 nearby galaxies with HST Cepheid distances that can be used to independently calibrate the TF relation, 8 currently also have 3.6-μm published total magnitudes (Dale et al. 2007). In **Figure 7*a–c***, we show the B-, I-, and H-band TF relations for the entire sample of currently available calibrating galaxies from Sakai et al. (2000). Their magnitudes have been corrected for inclination-induced extinction effects and their line widths have been corrected to edge-on. The scatter is ± 0.43, 0.36, and 0.36 mag for the B-, I-, and H-band relations, respectively; the outer lines follow the mean regression at $\pm 2\sigma$. If it holds up with further data, this intrinsic scatter means that to measure a distance good to 5%, say, using even the best of these TF relations, one would need to find a grouping of 16 galaxies in order to beat down the intrinsic rms scatter. In **Figure 7*d***, we show the mid-IR TF relation for the eight galaxies with Cepheid distances and published Infrared Array Camera observations, measured here at 3.6 μm. The gains are impressive. With the magnitudes not even corrected for any inclination effects, the scatter within this sample is found to be only ± 0.12 mag. Each of these galaxies entered the calibration with its own independently determined Cepheid-calibrated distance. If this correlation stands the test of time as additional calibrators enter the regression, using the mid-IR TF relation, a single galaxy could potentially yield a distance good to $\pm 5\%$. All TF galaxies, when observed in the mid-IR, would then individually become precision probes of large-scale structure, large-scale flows, and the Hubble expansion.

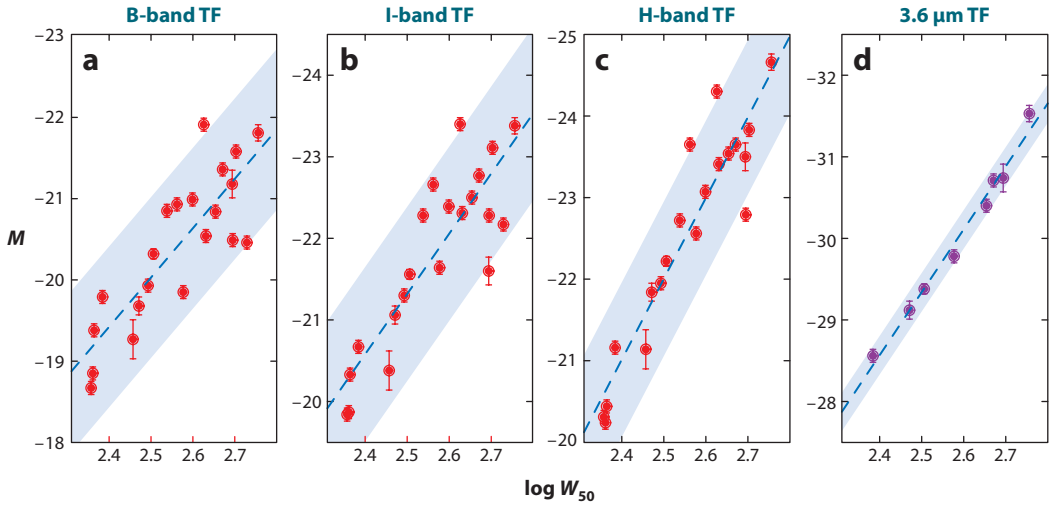

Figure 7

Multiwavelength Tully-Fisher (TF) relations. (*a–c*) The B-, I-, and H-band TF relations for all of the galaxies calibrated with independently measured Cepheid moduli from the *Hubble Space Telescope* Key Project. (*d*) The TF relation for the subset of galaxies drawn from the Key Project calibrators that also have published 3.6-μm total magnitudes. The significantly reduced dispersion in the mid-IR dataset is impressive; however, a larger sample of calibrators is needed to confirm the scatter and slope of the relation at this wavelength.

3.6. Type Ia Supernovae

One of the most accurate means of measuring cosmological distances out into the Hubble flow utilizes the peak brightness of SNe Ia. The potential of supernovae for measuring distances was clear to early researchers (e.g., Baade, Minkowski, Zwicky), but it was the Hubble diagram of Kowal (1968) that set the modern course for this field, followed by decades of work by Sandage, Tammann, and collaborators (e.g., Sandage & Tammann 1982, 1990; see also the review by Branch 1998). Analysis by Pskovskii (1984), followed by Phillips (1993), established a correlation between the magnitude of a SN Ia at peak brightness and the rate at which it declines, thus allowing supernova luminosities to be "standardized." This method currently probes farthest into the unperturbed Hubble flow, and it possesses very low intrinsic scatter: In recent studies, the decline-rate-corrected SN Ia Hubble diagram is found to have a dispersion of $\pm$ 7–10% in distance (e.g., Folatelli et al. 2010, Hicken et al. 2009). A simple lack of Cepheid calibrators prevented the accurate calibration of SNe Ia for determination of H_o prior to HST. Substantial improvements to the supernova distance scale have resulted from recent dedicated, ground-based supernova searches and follow-up programs yielding CCD light curves for nearby supernovae (e.g., Hamuy et al. 1996, Jha et al. 2006, Contreras et al. 2010). Sandage and collaborators undertook a major program with HST to find Cepheids in nearby galaxies that have been host to SNe Ia (Sandage et al. 1996, Saha et al. 1999), and thereby provided the first Cepheid zero-point calibration, which has recently been followed up by Macri et al. (2006) and Riess et al. (2009a,b).

For Hubble constant determinations, the challenge in using SNe Ia remains that few galaxies in which SN Ia events have been observed are also close enough for Cepheid distances to be measured. Hence, the calibration of the SN Ia distance scale is still subject to small-number statistical uncertainties. At present, the numbers of galaxies for which there are high-quality

Cepheid and SN Ia measurements (in most cases made with the same telescopes and instruments as the Hubble flow set) is limited to six objects (Riess et al. 2009b).

3.6.1. Underlying Theory. SNe Ia result from the thermonuclear runaway explosions of stars. From observations alone, the presence of SNe Ia in elliptical galaxies suggests that they do not come from massive stars. Many details of the explosion are not yet well understood, but the generally accepted view is that of a carbon-oxygen, electron-degenerate, nearly-Chandrasekhar-mass white dwarf orbiting in a binary system with a close companion (Whelan & Iben 1973). As material from the Roche lobe of the companion is deposited onto the white dwarf, the pressure and temperature of the core of the white dwarf increases until explosive burning of carbon and oxygen is triggered. An alternative model is that of a "double degenerate" system (merger with another white dwarf). Although on observational grounds, there appear to be too few white dwarf pairs, this issue has not been conclusively resolved. A review of the physical nature of SNe Ia can be found in Hillebrandt & Niemeyer (2000).

A defining characteristic of observed SNe Ia is the lack of hydrogen and helium in their spectra. It is presumed that the orbiting companion is transferring hydrogen- and helium-rich material onto the white dwarf; however, despite extensive searches, this hydrogen or helium has never been detected, and it remains a mystery as to how such mass transfer could take place with no visible signature. It is not yet established whether this is a problem of observational detection or whether these elements are lost from the system before the explosion occurs.

Various models for SN Ia explosions have been investigated. The most favored model is one in which a subsonic deflagration flame is ignited, which subsequently results in a supersonic detonation wave (a delayed detonation). The actual mechanism that triggers a SN Ia explosion is not well understood: Successfully initiating a detonation in a CO white dwarf remains extremely challenging. In recent years, modeling in 3D has begun, given indications from spectropolarimetry that the explosions are not spherically symmetric. The radiative transport calculations for exploding white dwarf stars are complex. However, there is general consensus that the observed (exponential shape of the) light curves of SNe Ia are powered by the radioactive decay of ^{56}Co to ^{56}Fe. The range of observed supernova peak brightnesses appears to be due to a range in ^{56}Ni produced. However, the origin of the peak magnitude–decline rate is still not well understood.

Despite the lack of a solid theoretical understanding of SNe Ia, empirically they remain one of the best-tested, lowest-dispersion, and highest-precision means of measuring relative distances out into the smooth Hubble flow.

3.6.2. Recent Results for Type Ia Supernovae and the Hubble Constant. The most recent calibration of SNe Ia has come from Riess et al. (2009a,b) from a new calibration of six Cepheid distances to nearby well-observed supernovae using the Advanced Camera for Surveys (ACS) and the Near-Infrared Camera and Multi-Object Spectrometer (NICMOS) on HST. Riess et al. have just completed a program to discover Cepheids in nearby galaxies known to have been hosts to relatively recent SNe Ia and then reobserved them in the near-IR. In so doing, the number of high-quality calibrators for the supernova distance scale more than doubled, putting the calibration for SNe Ia on a far more secure foundation. The six Cepheid-calibrated supernovae include SN1981B in NGC 4536, SN 1990N in NGC 4639, SN 1998aq in NGC 3982, SN 1994ae in NGC 3370, SN 1995al in NGC 3021, and finally SN 2002fk in NGC 1309. A comparison of Cepheid and SNe Ia distances from Riess et al. (2009b) is shown in **Figure 8**. The supernovae were chosen to meet rather stringent criteria, requiring, for example, that they all were observed with modern detectors, that they were observed before maximum light, that their spectra were not atypical, and

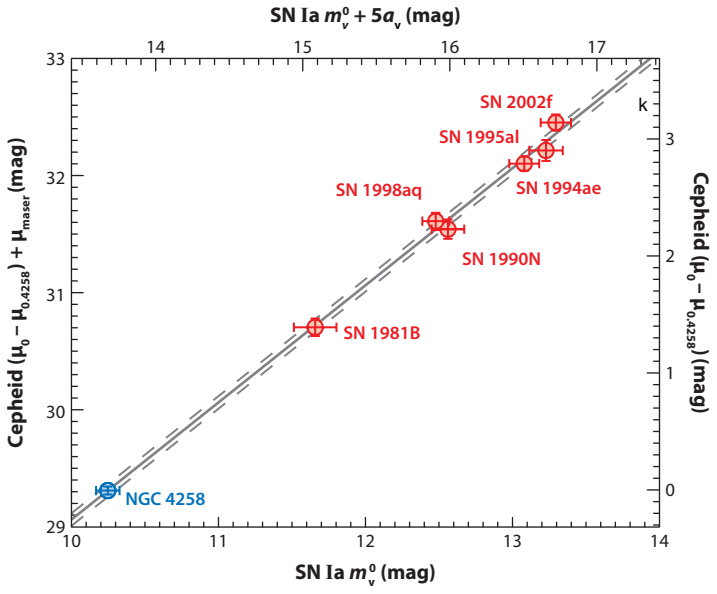

Figure 8

A comparison of Cepheid and Type Ia supernovae distances (*red points*), as described in Riess et al. (2009b). The calibrating galaxy, NGC 4258, is added in blue.

that their estimated reddenings were low. Each galaxy had between 13 and 26 Cepheids observed at random phases in the H band (F160W filter) (and were transformed to mean light using optical data) using NICMOS onboard HST. Extinction in the H band is down by a factor of five relative to the optical. The program avoids issues of cross-instrumental calibration by observing with a single telescope for the calibration galaxy, NGC 4258, out to the SNe Ia galaxies. By extending to the near-IR, these observations of the newly discovered Cepheids directly address the systematic effects of metallicity and reddening.

We show in **Figure 9** the Hubble diagram for 240 supernovae at $z < 0.1$ from Hicken et al. (2009), which have been calibrated by Riess et al. (2009b) based on the distance to the maser galaxy, NGC 4258. Riess et al. quote a value of $H_o = 74.2 \pm 3.6$ km s^{-1} Mpc^{-1} combining systematic and statistical errors into one number, a value in excellent agreement with that from the Key Project (see Section 4), which is calibrated using the Galactic Cepheid parallax sample. Currently, there is not much need for larger, low-redshift samples, because the dominant remaining uncertainties are systematic rather than statistical. Recent studies (e.g., Wood-Vasey et al. 2008, Folatelli et al. 2010) confirm that supernovae are better standard candles at near-IR (JHK) wavelengths and minimize the uncertainties due to reddening.

Tammann, Sandage & Reindl (2008) have undertaken a recent recalibration of supernovae, as well as a comparison of the Cepheid, RR Lyrae, and TRGB distance scales. In contrast, they find a value of $H_o = 62.3 \pm 4.0$ km s^{-1} Mpc^{-1}, where the quoted (systematic) error includes their estimated uncertainties in both the Cepheid and TRGB calibration zero points. Their quoted error is dominated by the systematic uncertainties in the Cepheid zero point and the small number of supernova calibrators, both of which are estimated by them to be at the 3–4% level; however, the H_o values differ by more than 2-σ. A discussion of the reason for the differences in these analyses can be found in Riess et al. (2009a,b): These include the use of more heavily reddened Galactic Cepheids, the use of less accurate photographic data, and a calibration involving multiple telescopes/instruments for supernovae by Tammann, Sandage & Reindl.

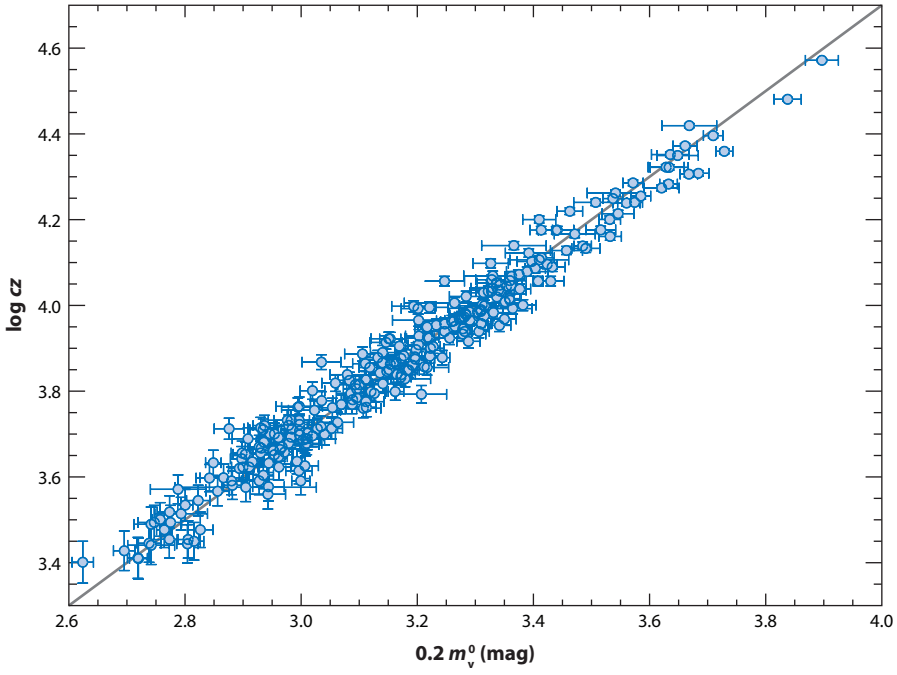

Figure 9

Supernova *Hubble* diagram based on 240 supernovae with $z < 0.1$. The sample is from Hicken et al. (2009) and has been used by Riess et al. (2009b) for their determination of H_o.

4. THE *HUBBLE SPACE TELESCOPE* KEY PROJECT

We briefly summarize below the results from the HST Key Project and provide an updated calibration for these data. The primary goals of the HST Key Project were to discover and measure the distances to 18 galaxies containing Cepheid variables, calibrate a range of methods for measuring distances beyond the reach of Cepheids to test for and minimize sources of systematic uncertainty, and ultimately to measure H_o to an accuracy of $\pm 10\%$ (Freedman et al. 2001). HST provided the opportunity to measure Cepheid distances a factor of 10 more distant than could be routinely obtained on the ground. It also presented a practical advantage in that, for the first time, observations could be scheduled in a way that optimized the discovery of Cepheids with a range of periods independent of the phase of the moon or the weather (Madore & Freedman 2005).

Cepheid distances to 18 galaxies with distances in the range of 3 to 25 Mpc were measured using WF/PC and (primarily) WFPC2 on HST. Observations at two wavelengths (*V*- and *I*-band) were made, which were chosen to allow corrections for dust. The spacing of observations was optimized to allow for the discovery of Cepheids with periods in the range of 10 to 50 days. In addition, 13 additional galaxies with published Cepheid photometry were analyzed for a total of 31 galaxies.

These Cepheid distances were then used to calibrate the TF relation for spiral galaxies, the peak brightness of Sne Ia, the $D_n-\sigma$ relation for elliptical galaxies, the SBF method, and Type II supernovae (Freedman et al. 2001 and references therein). These methods allowed a calibration of distances spanning the range of about 70 Mpc (for SBF) out to about 400 Mpc for Type Ia SNe. These results are summarized in **Figure 10**. Combining these results using both Bayesian and frequentist methods yielded a consistent value of $H_o = 72 \pm 3$ (statistical) ± 7 (systematic) km s^{-1} Mpc^{-1}.

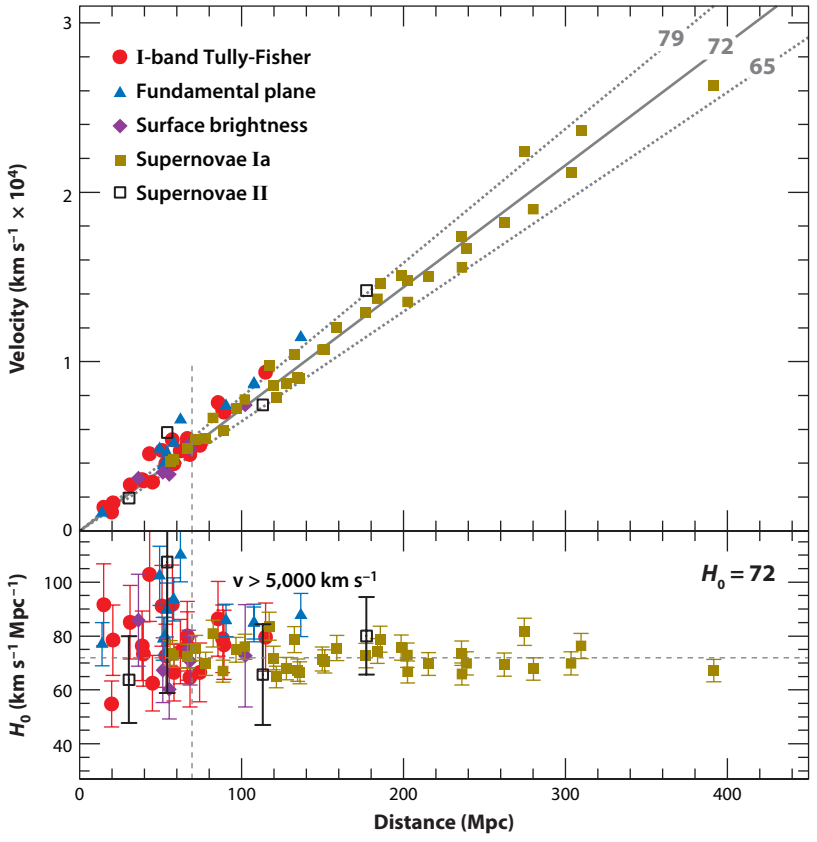

Figure 10

Graphical results of the *Hubble Space Telescope* Key Project (Freedman et al. 2001). (*Top*) The Hubble diagram of distance versus velocity for secondary distance indicators calibrated by Cepheids. Velocities are corrected using the nearby flow model of Mould et al. (2000). Dark yellow squares, Type Ia supernovae; filled red circles, Tully-Fisher (TF) clusters (I-band observations); blue triangles, fundamental plane clusters; purple diamonds, surface brightness fluctuation galaxies; open black squares, Type II supernovae. A slope of $H_o = 72 \pm 7$ km s^{-1} Mpc^{-1} is shown (*solid and dotted gray lines*). Beyond 5,000 km s^{-1} (*vertical dashed line*), both numerical simulations and observations suggest that the effects of peculiar motions are small. The Type Ia supernovae extend to about 30,000 km s^{-1}, and the TF and fundamental plane clusters extend to velocities of about 9,000 and 15,000 km s^{-1}, respectively. However, the current limit for surface brightness fluctuations is about 5,000 km s^{-1}. (*Bottom*) The galaxy-by-galaxy values of H_o as a function of distance.

We update this analysis using the new HST-parallax Galactic calibration of the Cepheid zero point (Benedict et al. 2007) and the new supernova data from Hicken et al. (2009). We find a similar value of H_o, but with reduced systematic uncertainty, of $H_o = 73 \pm 2$ (random) $\pm$ 4 (systematic) km s^{-1} Mpc^{-1}. The reduced systematic uncertainty, discussed further in Section 4.1 below, results from having a more robust zero-point calibration based on the Milky Way Galaxy with comparable metallicity to the spiral galaxies in the HST Key Project sample. Although, the new parallax calibration results in a shorter distance to the LMC (which is no longer used here as a calibrator), the difference in H_o is nearly offset by the fact that no metallicity correction is needed to offset the difference in metallicity between the LMC and calibrating galaxies.

4.1. Systematics on the Hubble constant at the End of the Key Project and a Decade Later

A primary goal of the HST Key Project was the explicit propagation of statistical errors combined with the detailed enumeration of and accounting for known and potential systematic errors. In **Table 2**, we recall the systematics error budget given in Freedman et al. (2001). The purpose of the original tabulation was to clearly identify the most influential paths to greater accuracy in future efforts to refine H_o. Here, we now discuss what progress has been made and what we can expect in the very near future using primarily space-based facilities utilizing instruments operating mainly at mid-IR and near-IR wavelengths.

Identified systematic uncertainties in the HST Key Project determination of the extragalactic distance scale limited its stated accuracy to $\pm 10\%$. The dominant systematics were (*a*) the zero point of the Cepheid PL relation, which was tied directly to the (independently adopted) distance to the LMC; (*b*) the differential metallicity corrections to the PL zero point in going from the relatively low-metallicity (LMC) calibration to target galaxies of different (and often larger) metallicities; (*c*) reddening corrections that required adopting a wavelength dependence of the extinction curve that is assumed to be universal; and (*d*) zero-point drift, offsets, and transformation uncertainties between various cameras on HST and on the ground. **Table 2** compares these uncertainties to what is now being achieved with HST parallaxes and new HST SNe Ia distances (see **Table 2**, Column 3, "Revisions"), and then what is expected to be realized by extending to a largely space-based near- and mid-IR Cepheid calibration using the combined power of HST, *Spitzer*, and eventually the *James Webb Space Telescope* (JWST) and GAIA. (see **Table 2**, Column 4, "Anticipated").

In 2001, the uncertainty on the zero point of the Leavitt Law was the largest on the list of known systematic uncertainties. Recall that the Key Project zero point was tied directly to an LMC true distance modulus of 18.50 mag. As we have seen in Section 3.1.4, improvement to the zero point has come from new HST parallax measurements of Galactic Cepheids, improved distance measurements to the LMC from near-IR photometry, and measurement of a maser distance to NGC 4258. We adopt a current zero-point uncertainty of 3%.

We next turn to the issue of metallicity. As discussed in Section 3.1.3, in the optical, metallicity corrections remain controversial. However, by shifting the calibration from the low-metallicity Cepheids in the LMC to the more representative and high-metallicity Milky Way or (alternatively to) the NGC 4258 Cepheids, the character of the metallicity uncertainty has changed from being a systematic to a random uncertainty. We conservatively estimate that the systematic component of the uncertainty on the metallicity calibration should now drop to ± 0.05 mag. Including the

Table 2 Systematics error budget on H_o: past, present, and future

Known	Key Project	Revisions	Anticipated	Basis
Systematics	(2001)	(2007/2009)	*Spitzer*/JWST	
(1) Cepheid Zero Point	± 0.12 mag	± 0.06 mag	± 0.03 mag	Galactic Parallaxes
(2) Metallicity	$\pm$ 0.10 mag	± 0.05 mag	± 0.02 mag	IR + Models
(3) Reddening	± 0.05 mag	± 0.03 mag	± 0.01 mag	IR 20–30 $\times$ Reduced
(4) Transformations	± 0.05 mag	± 0.03 mag	± 0.02 mag	Flight Magnitudes
Final Uncertainty	± 0.20 mag	± 0.09 mag	± 0.04 mag	Added in Quadrature
Percentage Error on H_o	$\pm 10\%$	$\pm 5\%$	$\pm 2\%$	Distances

Revisions (Column 2) incorporating the recent work of Benedict et al. (2007) and Riess et al. (2009b).

recent results from Benedict et al. (2007) and Riess et al. (2009a,b), our estimate for the current total uncertainty on H_o is $\pm 5\%$.

There has recently been discussion in the literature about possible variations in the slope of the Leavitt Law occurring around 10 days [see Ngeow, Kanbur & Nanthakumar (2008) and references therein]; however, Riess et al. (2009a) and Madore & Freedman (2009) both find that when using W, the differences are not statistically significant.

In terms of future improvements, as discussed further in Section 7, with the GAIA, and possibly the *Space Interferometry Mission* (SIM), the sample of Cepheids with high-precision trignometric parallaxes will be increased, and as more long-period Cepheids enter the calibration, both the slope and the zero point of the high-metallicity Galactic Leavitt Law will be improved. By extending both the calibration of the Leavitt Law and its application to increasingly longer wavelengths, the effects of metallicity, and the impact of total line-of-sight reddening, each drop below the statistical significance threshold. At mid-IR wavelengths, the extinction is reduced by a factor of $\sim$20 compared to optical wavelengths. In addition, line blanketing in the mid- and near-IR wavelengths is predicted theoretically to be small compared to the blue portion of the spectrum. Direct tests are now being undertaken to establish whether this is indeed the case and/or calibrate out any residual impact (see Section 7.3).

In principle, a value of H_o having a well-determined systematic error budget of only 2–3% is within reach over the next decade. It is the goal of the new Carnegie Hubble Program, described briefly in Section 7.3, which is based on a mid-IR calibration of the extragalactic distance scale using the *Spitzer* satellite, GAIA, and JWST.

5. OTHER METHODS FOR DETERMINING THE HUBBLE CONSTANT

Although the focus of this review is the determination of H_o and the extragalactic distance scale, we briefly mention two indirect techniques that probe great cosmological distances independently: gravitational lensing and the Sunyaev-Zel'dovich effect. We also discuss measurements of anisotropies in the cosmic microwave background (CMB), which offer a measurement of H_0 in combination with other data.

5.1. Gravitational Lens Time Delays and the Hubble Constant

As first realized by Refsdal (1964), measurements of the differences in arrival time, coupled with measurements of the angular separation of strongly lensed images of a time-variable object (such as a quasar or supernova) can be used to measure H_o. The time delay observed between multiple images is proportional to H_o^{-1}, and is less dependent on other cosmological parameters such as Ω_{matter} and Ω_Λ. An extensive review of the physics of lensing can be found in Blandford & Narayan (1992); the observational issues have been summarized nicely by Myers (1999) and Schechter (2005).

Initially, the practical implementation of this method suffered from a number of difficulties. Time delays have proven difficult to measure accurately, the amplitude of quasar variability is generally small, and relatively few lens systems that can be modeled simply and cleanly have been found. Dust obscuration is an issue at optical wavelengths. A great challenge of this method is that astronomical lenses are galaxies whose underlying mass distributions are not known, and a strong physical degeneracy exists between the mass distribution of the lens and the value of H_o. As emphasized by Gorenstein, Shapiro & Falco (1988), the deflections and distortions do not uniquely determine the mass distribution: A lens may be located in a group(s) or cluster(s), which will affect the predicted time delays, an effect termed the mass sheet degeneracy. Measurements of

velocity dispersion as a function of position can be used to constrain the mass distribution of the lens, but generally only central velocity dispersion measurements are feasible. An advantage of the method is that it offers a probe directly at cosmological distances; the concomittent disadvantage is that the cosmological model must be assumed in order to determine H_o. Earlier estimates of H_o using this technique yielded values about 10% lower (analyzing the same data), assuming what was then the standard cosmological model with $\Omega_{matter} = 1.0$, as compared to the current standard model with $\Omega_{matter} = 0.3$ and $\Omega_\Lambda = 0.7$.

The precision and accuracy of this technique has continued to improve over time. A brief survey of results from gravitational lensing over the past five years can be found in Suyu et al. (2009), with estimates of H_o in the range of 50 to 85 km s^{-1} Mpc^{-1}. There is a wide range in types of modeling and treatment of errors for these different systems (e.g., assumed isothermal profiles, assumptions about the density distribution of the environment, and how well the models are constrained by the data).

A recent extensive analysis of the quadruple lens system B1608+656 has been carried out by Suyu et al. (2009). This analysis is based on deep F606W and F814W ACS data, a more accurate measurement of the velocity dispersion using the Low-Resolution Imaging Spectrometer (LRIS) on Keck, a more detailed treatment of the lens environment using a combination of ray tracing through cosmological N-body simulations (the Millennium Simulation) along with number counts in the field of B1608+656 in order to help break the mass sheet degeneracy problem. Adopting the standard cosmological model with $\Omega_{matter} = 0.3$, $\Omega_\Lambda = 0.7$, and $w = -1$, they find $H_o = 71 \pm 3$ km s^{-1} Mpc^{-1}, a factor of two improvement over the previous estimate for this lens.

5.2. The Sunyaev-Zel'dovich Effect and the Hubble Constant

Sunyaev & Zel'dovich (1969) described the inverse-Compton scattering of photons from the CMB off of hot electrons in the X-ray gas of rich clusters of galaxies. This scattering leads to a redistribution of the CMB photons so that a fraction of the photons move from the Rayleigh-Jeans to the Wien side of the blackbody spectrum, referred to as the Sunyaev-Zel'dovich (SZ) effect. The measured effect amounts to about 1 mK. The Hubble constant is obtained using the fact that the measured X-ray flux from a cluster is distance-dependent, whereas the SZ decrement is essentially independent of distance. Observations of this effect have improved enormously in recent years, with high signal-to-noise, high angular resolution, SZ images obtained with ground-based interferometric arrays and high-resolution X-ray spectra. The theory of the SZ effect is covered at length by Birkinshaw (1999); a nice summary of observational techniques and interferometry results is given in Carlstrom, Holder & Reese (2002).

The SZ effect is proportional to the first power of the electron density, n_e: $\Delta T_{SZ} \sim \int dl n_e T_e$, where T_e is the electron temperature, and dl is the path length along the line of sight, which is related to the angular diameter distance. The X-ray emission is proportional to the second power of the density: $S_x \sim \int dl \Lambda n_e^2$, where Λ is the cooling function for the X-ray gas. The angular diameter distance is solved for by eliminating the electron density (see Carlstrom, Holder & Reese 2002; Birkinshaw 1999).

An advantage of this method is that it can be applied at cosmological distances, well into the Hubble flow. The main uncertainties result from potential substructure in the gas of the cluster (which has the effect of reducing H_o), projection effects (if the clusters observed are prolate, the sense of the effect is to increase H_o), the assumption of hydrostatic equilibrium, details of the models for the gas and electron densities, and potential contamination from point sources.

The accuracy of this technique has continued to improve as interferometric radio observations, e.g., Berkeley-Illinois-Maryland Association (BIMA) and Owens Valley Radio Observatory

(OVRO), and ROSAT and now *Chandra X-ray Observatory* data have become available. In a recent study by Bonamente et al. (2006), new *Chandra* X-ray measurements for 38 clusters in the redshift range of $0.14 < z < 0.89$ have been obtained. Combining these data with BIMA and OVRO data for these same clusters, and performing a Markov Chain Monte Carlo analysis, these researchers find a value of $H_o = 76.9^{+3.9+10.0}_{-3.4-8.0}$ km s^{-1} Mpc^{-1}, assuming hydrostatic equilibrium. Relaxing the assumption of hydrostatic equilibrium, and adopting an isothermal β model, they find $H_o = 73.7^{+4.6+9.5}_{-3.8-7.6}$ km s^{-1} Mpc^{-1}.

5.3. Measurements of Anisotropies in the Cosmic Microwave Background

The prediction of acoustic oscillations in CMB radiation (Peebles & Yu 1970, Sunyaev & Zel'dovich 1970) and the subsequent measurement of these peaks have culminated most recently in the five-year measurements of WMAP (Dunkley et al. 2009), which is one of the most successful chapters in the history of cosmology. A recent detailed review of the CMB is given in Hu & Dodelson (2002). The aim in this Section is simply to elucidate the importance of accurate measurements of the Hubble constant in the context of measurements of the angular power spectrum of CMB anisotropies and the complementary nature of the constraints provided.

The temperature correlations in the maps of the CMB can be described by a set of spherical harmonics. A plot of the angular power spectrum as a function of multipole moment, l, is shown in **Figure 11**. This spectrum can be naturally explained as a result of the tight coupling between photons and baryons before recombination (when electrons and protons combine to form neutral

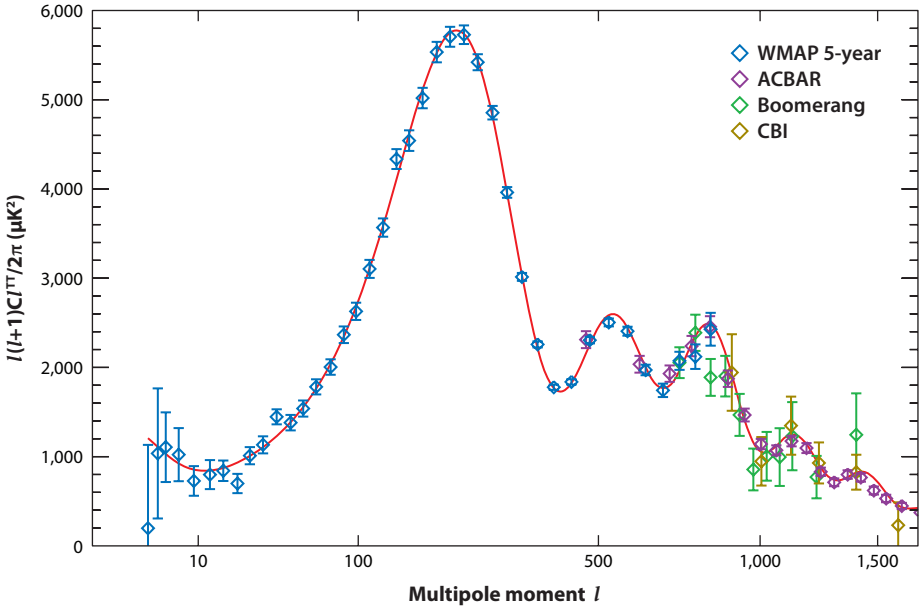

Figure 11

The *Wilkinson Microwave Anisotropy Probe* (WMAP) 5-year "temperature angular power spectrum" (*blue data points*) (Nolta et al. 2009), incorporating other recent results from the ACBAR (Arcminute Cosmology Bolometer Array Receiver) (*purple*, Reichardt et al. 2009), Boomerang (Balloon Observations of Millimetric Extragalactic Radiation and Geophysics) (*green*, Jones et al. 2006), and CBI (Cosmic Background Imager) (*dark yellow*, Readhead et al. 2004) experiments. The red curve is the best-fit cold dark matter model to the WMAP data.

hydrogen), and a series of oscillations are set up as gravity and radiation pressure act on the cold dark matter and baryons. After recombination, photons free-stream toward us. The position of the first peak in this diagram is a projection of the sound horizon at the time of recombination and occurs at a scale of about 1°.

Although measurements of the CMB power spectrum can be made to very high statistical precision, there are some nearly exact degeneracies that limit the accuracy with which cosmological parameters can be estimated (e.g., Efstathiou & Bond 1999). These degeneracies impose severe limitations on estimates of curvature and the Hubble constant derived from CMB anisotropy alone and are sometimes overlooked. Specifically, the value of H_o is degenerate with the value of Ω_Λ and w. Different combinations of the matter and energy densities and H_o can produce identical CMB anisotropy spectra. Alternatively, an accurate independent measurement of H_o provides a means of constraining the values of other cosmological parameters based on CMB anisotropy data.

The WMAP data provide strong evidence for the current standard cosmological model with $\Omega_{matter} = 0.23$ and $\Omega_\Lambda = 0.73$ (Spergel et al. 2003, Komatsu et al. 2009). A prior on H_o can help to break some of the degeneracies in the CMB data. The WMAP data measure $\Omega_{matter}h^2$; assuming a flat universe yields a stronger constraint on the equation of state, -0.47, $w < 0.42$ (95% CL) (Komatsu et al. 2009) than WMAP data alone. Alternatively, combining the WMAP-5-year data with SNe Ia and baryon acoustic oscillations (BAOs) data yields a value of $H_o = 70.5 \pm 1.3$ km s^{-1} Mpc^{-1} (Komatsu et al. 2009), which is still in excellent agreement with other methods.

5.3.1. Measurements of Baryon Acoustic Oscillations in the Matter Power Spectrum. Baryon acoustic oscillations arise for the same underlying physical reason as the peaks and valleys in the CMB spectrum: The sound waves that are excited in the hot plasma owing to the competing effects of radiation pressure and gravity at the surface of last scattering also leave an imprint on the galaxy matter power spectrum. The two-point correlation function has a peak on scales of 100 h^{-1} Mpc (Eisenstein et al. 2005), which provides a "standard ruler" for measuring the ratio of distances between the surface of last scattering of the CMB (at $z = 1089$) and a given redshift. Measurement of BAOs in the matter power spectrum can also help to break degeneracies in the CMB measurements. For example, Percival et al. (2009) have combined the Sloan Digital Sky Survey (SDSS) seventh data release with the Two-degree Field Galaxy Redshift Survey (2dFGRS) to measure fluctuations in the matter power spectrum at six redshift slices. For ΛCDM models, combining these results with constraints for the baryon and cold dark matter densities, $\Omega_b h^2$ and $\Omega_{CDM} h^2$ from WMAP 5, and data for SNe Ia yields $\Omega_{matter} = 0.29 \pm 0.02$ and $H_o = 68 \pm 2$ km s^{-1} Mpc^{-1}.

6. AGE OF THE UNIVERSE

There are three independent ways of determining the age of the Universe. The first is based on an assumed cosmological model and the current expansion rate of the Universe. The second is based on models of stellar evolution applied to the oldest stars in the Universe. The third is based on measurements of the angular power spectrum of temperature fluctuations in the CMB. All three methods are completely independent of each other and so offer an important consistency check. The kinematic age of the Universe is governed by the rate at which the Universe is currently expanding, modified by the combined extent to which gravity slows the expansion and dark energy causes it to accelerate.

The time back to the Big Bang singularity depends upon H_o and the expansion history, which itself depends upon the composition of the Universe:

$$t_o = \int_0^\infty \frac{dz}{(1+z)H(z)} = H_o^{-1} \int_0^\infty \frac{dz}{(1+z)[\Omega_{matter}(1+z)^3 + \Omega_{DE}(1+z)^{3(1+w)}]^{1/2}}. \quad (14)$$

For a matter-dominated flat universe with no dark energy ($\Omega_{matter} = 1.0$, $\Omega_{vacuum} = 0.0$), the age is simply two-thirds of the Hubble time or only 9.3 billion years for $h = 0.7$.

Not accounting for the presence of dark energy in the Universe leads to an underestimate of its age. Before the discovery of dark energy, an "age controversy" persisted for several decades: Values of the Hubble constant any larger than 40–50 km s^{-1} Mpc^{-1} appeared to yield ages for the Universe as a whole that were smaller than stellar-evolution-calibrated ages of the oldest stars in the Milky Way. For a universe with a Hubble constant of 73 km sec^{-1} Mpc^{-1}, with $\Omega_{matter} = 0.27$ and $\Omega_{vacuum} = 0.73$, the age is 13.3 Gyr. Taking account of the systematic uncertainties in H_o alone, the uncertainty in the age of the Universe is estimated to be about ± 0.8 Gyr.

The most well-developed of the stellar chronometers employs the oldest stars in globular clusters in the Milky Way (Krauss & Chaboyer 2003). The largest uncertainty for this technique comes from determination of the distances to the globular clusters. Recently, detailed stellar evolution models, when compared to observations of globular clusters stars, yield a lower limit to their ages of 10.4 billion years (at the 95% confidence level) with a best-fit age of 12.6 Gyr. Deriving the age for the Universe from the lower limit requires allowing for additional time to form the globular clusters: From theoretical considerations, this is estimated to be about 0.8 billion years. This age estimate for the Universe agrees well with the expansion age. Two other stellar chronometers—the cooling of the oldest white dwarf stars (for a recent review see Moehler & Bono 2008) and nucleocosmochronology, the decay of radioactive isotopes (Sneden et al. 2001)—yield similar ages.

The expansion age can also be determined from measurements of the CMB anisotropy. H_o cannot be measured directly from the CMB alone, but the heights of the peaks in the CMB spectrum provide a constraint on the product $\Omega_{matter} H_o^2$, and the position of the peaks constrain the distance to the last-scattering surface. Assuming a flat universe yields a consistent age, $t_o = 13.7 \pm 0.13$ Gyr (Spergel et al. 2003, Komatsu et al. 2009), again in good agreement with the other two techniques.

In summary, several methods of estimating the age of the Universe are now in good agreement, to within their quoted uncertainties, with a value of $t_o = 13.7 \pm 0.5$ Gyr.

7. WHY MEASURE THE HUBBLE CONSTANT TO HIGHER ACCURACY?

The importance of pinning down H_o has only grown with time: Not only does it set the scale for all cosmological distances and times, but its accurate determination is also needed to take full advantage of the increasingly precise measurements of other cosmological quantities. The prospects for improving the accuracy of H_o within the next decade appear to be as exciting as those within the past couple of decades. We highlight here near-term improvements to the Cepheid-based extragalactic distance scale that will come from new measurements of Cepheid parallaxes with GAIA and perhaps SIM; *Spitzer* measurements of Cepheids in the Milky Way, LMC, and other nearby galaxies, including NGC 4258; *Spitzer* measurements of the TF relation and a new calibration of the Type Ia supernova distance scale; and future measurements of Cepheids with JWST. We describe how a more accurate value of H_o, combined with other future measurements of large-scale structure and CMB anisotropies (e.g., Planck), can be used to break degeneracies and place stronger constraints on other cosmological parameters including the equation of state for dark energy, the energy density in cold dark matter, and the mass of neutrinos.

Although measurements of CMB anisotropies have provided dramatic confirmation of the standard concordance model, it is important to keep in mind that the values for many quantities (e.g., w, H_o, neutrino masses) are highly model-dependent owing to the strong degeneracies. A more accurate, independent measurement of H_o is critical for providing stronger limits on quantities such as w and neutrino masses.

7.1. Constraints on Dark Energy

As summarized by Hu (2005), a measurement of H_o to the percent level, in combination with CMB measurements with the statistical precision of the Planck satellite, offers one of the most precise measurements of the equation of state at $z \sim 0.5$. At first this result appears counterintuitive, because the CMB anisotropies result from physical processes imprinted on the surface of last scattering at $z \sim 1{,}100$. Alone they give very little information on dark energy, which contributes most to the expansion at lower redshifts. However, the sound horizon provides a reference standard ruler that can be used to provide constraints on a number of parameters including dark energy and neutrinos. The main deviations in the Hubble parameter, the angular diameter distance, and the growth factor due to the dark energy equation of state manifest themselves as variations in the local Hubble constant. In **Figure 12**, we show the strong degeneracy between the equation of state and the value of H_o. This figure is based on a forecast of the precision that will be available with measurements of CMB fluctuations from the Planck satellite. Improved accuracy in the measurement of H_o will be critical for constraining the equation of state for dark energy from CMB data.

7.2. Constraints on the Neutrino Mass

Improved accuracy in the measurement of H_o will have a significant effect in placing constraints on the neutrino mass from measurements of CMB anisotropies. Detailed reviews of the subject can be found in Dolgov (1996); Crotty, Lesgourges & Pastor (2004); and Hannestad (2006). Briefly, massive neutrinos contribute to the overall matter density of the Universe through which they have an impact on the growth of structure; the larger the neutrino mass, the more free-streaming effects dampen the growth of structure on small scales. The density in neutrinos is related to the number of massive neutrinos, N_{eff}, and the neutrino mass, m_ν, by $\Omega_\nu h^2 = N_{eff} m_\nu / 94$ eV. From neutrino oscillation experiments, a measurement of the difference in mass squared, $\Delta m^2 \sim 0.002$ $(\text{eV})^2$, is obtained.

In the context of the standard cosmological model, cosmological observations can constrain the number of neutrino species and the absolute mass scale. Massive neutrinos have a measurable effect on the CMB spectrum: The relative height of the acoustic peaks decrease with increasing m_ν and the positions of the peaks shift to higher multipole values. The WMAP 5-year data provided evidence, for the first time, for a nonzero neutrino background from CMB data alone, with $\sum m_\nu < 1.3$ eV (95% CL) (Dunkley et al. 2009). Combining the CMB data with results from SNe Ia and BAO results in a bound of $\sum m_\nu < 0.58$ eV (95% CL) (Komatsu et al. 2010), reaching close to the range implied by the neutrino oscillation experiments. Future forecasts with Planck data suggest that an order-of-magnitude increase in accuracy may be feasible.

One of the biggest limitations to determining the neutrino mass from the CMB power spectrum results from a strong degeneracy between the neutrino mass and the Hubble constant (Komatsu et al. 2009). As H_o increases, the neutrino mass becomes smaller (see **Figure 13**). An accuracy in H_o to 2–3% percent, combined with Planck data (for the standard cosmological model), will provide an order-of-magnitude improved precision on the neutrino mass.

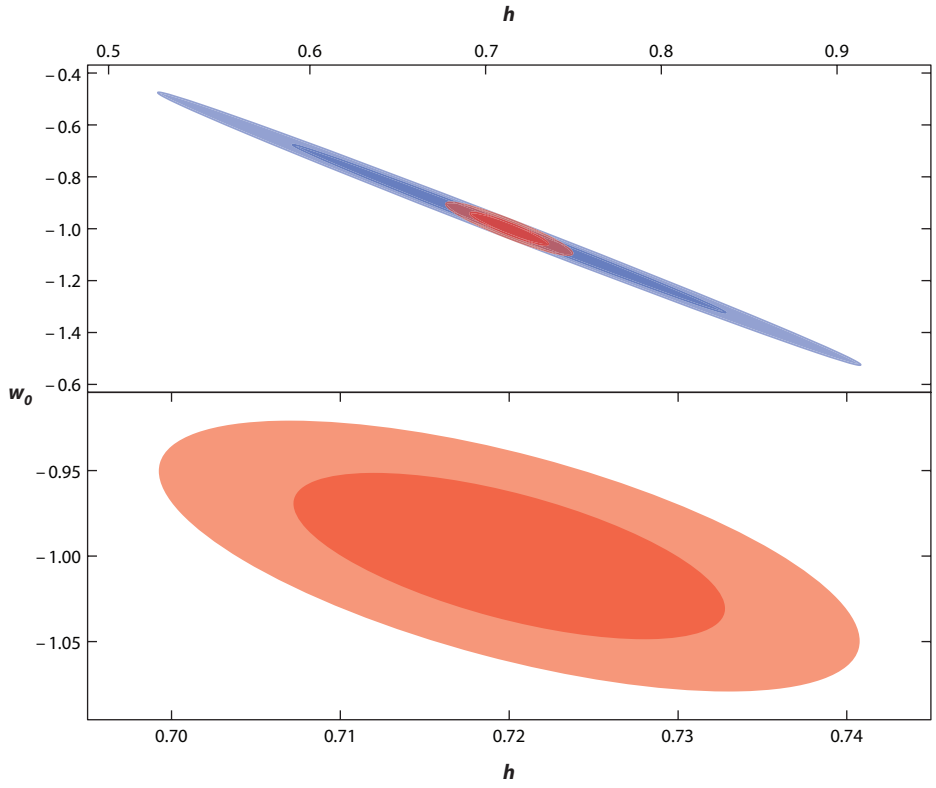

Figure 12

(*Top*) A plot illustrating the degeneracies of w_o with $h = (H_o/100)$, assuming the statistical uncertainties expected for the *Planck* satellite, a flat universe ($\Omega_k = 0$), and constant dark energy ($w_a = 0$). The plot uses the *Planck* Fisher matrix from the DETFast software package (Albrecht et al. 2006) The outer blue contours show the 68% and 95% confidence intervals from the H_o Key Project ($h = 0.72 \pm 0.08$), and the inner red contours show the case for a 2% uncertainty in H_o. Improved precision in H_o will allow an accurate measurement of w from the cosmic microwave background independent of other methods. (*Bottom*) Same as above, adding in constraints from Stage III supernovae and baryon acoustic oscillation experiments, as described in Albrecht et al. (2006).

7.3. Measuring the Hubble Constant to ±2%

Accuracy in measurement of H_o has improved signficantly with the measurement of HST Galactic Cepheid parallaxes and HST measurement of Cepheid distances to SNe Ia hosts, as described in Sections 3.1.4 and 3.5.2, respectively. Future improvements will come with further HST Wide Field Camera 3 and *Spitzer* observations of Cepheids. At 3.6 and 4.5 μm, the effects of extinction are a factor of ∼20 smaller in comparison to optical wavelengths. In addition, in the mid-IR, the surface brightness of Cepheids is insensitive to temperature. The amplitudes of the Cepheids are therefore smaller and due to radius variations alone. The Leavitt Law in the mid-IR then becomes almost equal to the period-radius relation. From archival *Spitzer* data, the mid-IR Leavitt Law has been shown to have very small dispersion (Freedman et al. 2008; Madore et al. 2009). Furthermore, metallicity effects are expected to be small in the mid-IR, and *Spitzer* offers an opportunity to test this expectation empirically. The calibration can be carried out using *Spitzer* alone, once again eliminating cross-calibration uncertainties. A new program aimed at addressing

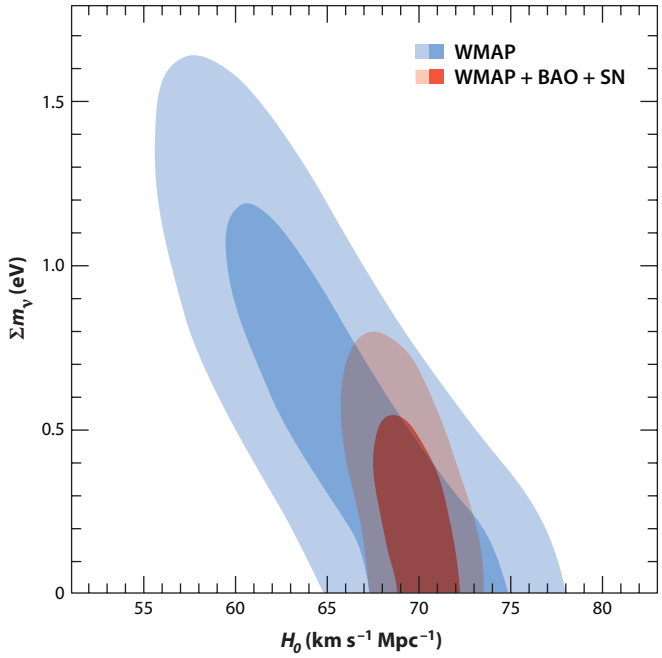

Figure 13

Wilkinson Microwave Anisotropy Probe 5-year (WMAP5) data showing the degeneracy between the sum of neutrino masses and H_o (from figure 17 of Komatsu et al. 2009). The blue contours show the WMAP5 data only (68% and 95% CL); the red contours include baryon acoustic oscillation and Type Ia Sne data.

remaining systematic errors in the Cepheid distance scale is the Carnegie Hubble Program (CHP) (Freedman 2009).

The CHP will measure the distances to 39 Galactic Cepheids (15 of them in anticipation of the GAIA satellite); 92 well-observed Cepheids in the LMC; several Local Group galaxies containing known Cepheids (M31, M33, IC 1613, NGC 6822, NGC 3109, Sextans A, Sextans B, and WLM); more distant galaxies with known Cepheids including NGC 2403 (2.5 Mpc); Sculptor Group galaxies NGC 300 and NGC 247 (3.7 Mpc); Cen A (3.5 Mpc) and M83 (4.5 Mpc); as well as the maser galaxy NGC 4258 (at 7.2 Mpc). It will measure the distances to 545 galaxies in 35 clusters with measured TF distances, which can then be calibrated with Cepheids as shown in **Figure 7**. Over 50 galaxies with SNe Ia distances measured by Folatelli et al. (2010) will also be observed as part of this program, allowing the determination of H_o with this calibration out into the far-field Hubble flow.

As discussed earlier, the expected uncertainties from the CHP are shown in **Table 2**. Reobserving the known Cepheids in more distant galaxies will require the aperture, sensitivity, and resolution of JWST. With *Spitzer*, it will be possible to decrease the uncertainties in the Cepheid distance scale to the 3–4% level, with an application of a new mid-IR TF relation and a *Spitzer* Cepheid calibration of Type Ia SNe. It is expected that future JWST measurements will bring the uncertainties to $\pm 2\%$ with a more firm calibration of SNe Ia.

FUTURE IMPROVEMENTS

We summarize here the steps toward measuring the Hubble constant to a few percent accuracy. Most of these measurements should be feasible within the next decade.

1. Mid-IR Galactic Cepheid parallax calibration with *Spitzer* and GAIA.
2. Mid-IR calibrations of Galactic and nearby Cepheid galaxies and the IR TF relation with *Spitzer* and JWST.
3. Increased numbers of maser distances.
4. Larger samples and improved systematics and modeling of strong gravitational lenses and Sunyaev-Zel'dovich clusters.
5. Higher frequency, greater sensitivity, higher angular resolution measurements of the CMB angular power spectrum with Planck.
6. Measurements of baryon acoustic oscillations at a range of redshifts (e.g., BOSS, **http://cosmology.lbl.gov/BOSS/**; HETDEX, **http://hetdex.org/**; WiggleZ, **http://wigglez.swin.edu.au/site/**; JDEM, **http://jdem.gsfc.nasa.gov/**; SKA, **http://www.skatelescope.org/**; DES, **http://www.darkenergysurvey.org/**; PanStarrs, **http://pan-starrs.ifa.hawaii.edu/public/**; LSST, **http://www.lsst.org/lsst**).
7. Beyond 2020, detection of gravitational radiation from inspiraling massive black holes with *Laser Interferometer Space Antenna*. Coupled with an identification of an electromagnetic source, and therefore a redshift, this method offers, in principle, a 1% measurement of H_o.

SUMMARY POINTS

1. Several nearby distance determination methods are now available that are of high precision, having independent systematics. These include Cepheid variables, the tip of the red giant branch (TRGB) stars, and the geometrically determined distances to maser galaxies.
2. The Cepheid period-luminosity relation (Leavitt Law) now has an absolute calibration based on HST trigonometric parallaxes for Galactic Cepheids. This calibration and its application at near-IR wavelengths significantly reduces two of the four leading systematic errors previously limiting the accuracy of the Cepheid-based distance scale: zero-point calibration and metallicity effects.
3. The maser galaxy distances, TRGB distances and Cepheid distances agree to high precision at the one common point of contact where they can each be simultaneously intercompared, the maser galaxy NGC 4258, at a distance of 7.2 Mpc.
4. Galactic Cepheid parallax and NGC 4258 maser calibrations of the distance to the LMC agree very well. Based on these and other independent measurements, we adopt a true, metallicity-corrected distance modulus to the LMC of 18.39 ± 0.06 mag.
5. HST optical and near-IR observations of Cepheids in SNe Ia galaxies calibrated by the maser galaxy, NGC 4258, have decreased systematics due to calibration, metallicity, and reddening in the SNe Ia distance scale, and increased the number of well-observed SN calibrators to six.
6. The current calibration of the Cepheid and maser extragalactic distance scales agree to within their quoted errors, yielding a value of $H_o = 73 \pm 2$ (random) $\pm$ 4 (systematic) km s^{-1} Mpc^{-1}.
7. Within a concordance cosmology (that is, $\Omega_{matter} = 0.27$ and $\Omega_{vacuum} = 0.73$), the current value of the Hubble constant gives an age for the Universe of 13.3 ± 0.8 Gyr. Several independent methods (globular cluster ages, white dwarf cooling ages, CMB anisotropies within a concordance model) all yield values in good agreement with the expansion age.

8. Further reductions of the known systematics in the extragalactic distance scale are anticipated using HST, *Spitzer*, GAIA, and JWST. A factor of two decrease in the currently identified systematic errors is within reach, and an uncertainty of 2% in the Hubble constant is a realistic goal for the next decade.
9. A Hubble constant measurement to a few percent accuracy, in combination with measurements of anisotropies in the CMB from Planck, will yield valuable constraints on many other cosmological parameters, including the equation of state for dark energy, the mass of neutrinos, and the curvature of the Universe.

DISCLOSURE STATEMENT

The authors are not aware of any affiliations, memberships, funding, or financial holdings that might be perceived as affecting the objectivity of this review.

ACKNOWLEDGMENTS

We thank the Carnegie Institution for Science, which, through its support of astronomical facilities and research for over a century, enabled the original discovery of the expansion of the Universe, as well as continued efforts to measure accurately the expansion of the Universe over cosmic time. Many dedicated individuals have made contributions to solving the problems encountered in accurately calibrating the extragalactic distance scale; it has been a community effort spanning the better part of a century, but it remained a problem that could not have been solved without NASA and its vision in supporting space astrophysics. We thank Chris Burns for producing **Figure 12**. We also thank Fritz Benedict, Laura Ferrarese, Robert Kirshner, James Moran, Jeremy Mould, and Adam Riess for their many constructive suggestions on an earlier draft of this review. Finally, our sincere thanks to John Kormendy, our ARAA Editor, for his patience and his insightful and helpful comments on the final version of this review as it went to press.

LITERATURE CITED

Aaronson M, Bothun G, Mould J, Huchra J, Schommer RA, Cornell ME. 1986. *Ap. J.* 302:536
Aaronson M, Huchra J, Mould JR. 1979. *Ap. J.* 229:1
Albrecht A, Bernstein G, Cahn R, Freedman WL, Hewitt J, et al. 2006. Report of the dark energy task force. (astro-ph/0609591)
Alcock C, Allsman RA, Alves DR, Axelrod TS, Basu A, et al. 2000. *Astron. J.* 119:2194
Baade W. 1944. *Ap. J.* 100:137
Barnes T. 2010. In *Stellar Pulsation: Challenges for Theory and Observation*, ed. J Guzik, P Bradley. *AIP Conf. Proc.* 1170:3
Bellazzini M. 2008. *Mem. Soc. Astron. Ital.* 79:440
Benedict GF, McArthur BE, Feast MW, Barnes TG, Harrison TE, et al. 2007. *Ap. J.* 79:453
Birkinshaw M. 1999. *Phys. Rep.* 310:97
Biscardi I, Raimondo G, Cantiello M, Brocato E. 2008. *Ap. J.* 678:168
Blakeslee JP, Lucey JR, Tonry JL, Hudson MJ, Narayanan VK, et al. 2002. *MNRAS* 330:443
Blakeslee JP, Jordan A, Mei S, Cote P, Ferrarese L, et al. 2009. *Ap. J.* 694:556
Blandford RD, Narayan R. 1992. *Annu. Rev. Astron. Astrophys.* 30:311
Bonamente M, Joy MK, LaRoque SJ, Carlstrom JE, Reese ED, et al. 2006. *Ap. J.* 647:25
Bono G, Caputo F, Fiorentino G, Marconi M, Musella I. 2008. *Ap. J.* 684:102
Branch D. 1998. *Annu. Rev. Astron. Astrophys.* 36:17

Buchler JR. 2010. In *Stellar Pulsation: Challenges for Theory and Observation*, ed. J Guzik, P Bradley. *AIP Conf. Proc.* 1170:51
Caldwell N. 2006. *Ap. J.* 651:822
Caputo F. 2008. *Mem. Soc. Astron. Ital.* 79:453
Cardelli JA, Clayton GG, Mathis JS. 1989. *Astron. J.* 96:695
Carlstrom JE, Holder GP, Reese ED. 2002. *Annu. Rev. Astron. Astrophys.* 40:643
Ciardullo R, Feldmeier JJ, Jacoby GH, Kuzio de Naray R, Laychak MB, et al. 2002. *Ap. J.* 577:31
Contreras C, Hamuy M, Phillips MM, Folatelli G, Suntzeff NB, et al. 2010. *Astron. J.* 139:519
Cox JP. 1980. *Theory of Stellar Pulsation*. Princeton: Princeton Univ. Press
Crotty P, Lesgourges J, Pastor S. 2004. *Phys. Rev. D* 69:3007
Da Costa GS, Armandroff TE. 1990. *Astron. J.* 100:162
Dale DA, Gil de Paz A, Gordon KD, Hanson HM, Armus L, et al. 2007. *Ap. J.* 655:863
di Benedetto GP. 2008. *MNRAS* 390:1762
Dessart L, Hiller DJ. 2005. *Astron. Astrophys.* 439:671
Dodelson S. 2003. *Modern Cosmology*. Amsterdam (Netherlands): Academic
Dolgov AD. 1996. *Nucl. Phys. B (Proc. Suppl.)* 48:5
Draine BT. 2003. *Annu. Rev. Astron. Astrophys.* 41:241
Durrell PR, Williams BF, Ciardullo R, Feldmeier JJ, von Hippel T, et al. 2007. *Ap. J.* 656:746
Dunkley J, Komatsu E, Nolta MR, Spergel DN, Larson D, et al. 2009. *Ap. J. Suppl.* 180:306
Efstathiou G, Bond JR. 1999. *MNRAS* 304:75
Eisenstein DJ, Zehavi I, Hogg DW, Scoccimarro R, Blanton MR, et al. 2005. *Ap. J.* 633:560
Feast MW, Catchpole RM. 1997. *MNRAS* 286:L1
Fernie JD. 1969. *Publ. Astron. Soc. Pac.* 81:707
Folatelli G, Phillips MM, Burns CR, Contreras C, Hamuy M, et al. 2010. *Astron. J.* 139:120
Fouque P, Arriagada P, Storm J, Barnes TG, Nardetto N, et al. 2007. *Astron. Astrophys.* 476:73
Freedman WL. 2009. *Bull. Am. Astr. Soc.* 41:710
Freedman WL, Madore BF. 1990. *Ap. J.* 365:186
Freedman WL, Madore BF, Gibson BK, Ferrarese L, Kelson DD, et al. 2001. *Ap. J.* 553:47
Freedman WL, Madore BF, Rigby J, Persson SE, Sturch L. 2008. *Ap. J.* 679:71
Giovanelli R, Haynes MP, Herter T, Vogt NP, da Costa LN, et al. 1997. *Astron. J.* 113:53
Gorenstein MV, Shapiro II, Falco EE. 1988. *Ap. J.* 327:693
Hamuy M, Phillips MM, Suntzeff NB, Schommer RA, Maza J, et al. 1996. *Astron. J.* 112:2398
Hannestad S. 2006. *Prog. Part. Nuc. Phys.* 57:309
Herrnstein JR, Moran JM, Greenhill LJ, Diamond PJ, Inoue M, et al. 1999. *Nature* 400:539
Hicken M, Wood-Vasey WM, Blondin S, Challis P, Jha S, et al. 2009. *Ap. J.* 700:1097
Hillebrandt W, Niemeyer JC. 2000. *Annu. Rev. Astron. Astrophys.* 38:191
Hodge P. 1982. *Annu. Rev. Astron. Astrophys.* 19:357
Hu W. 2005. *Observing Dark Energy* 339:215
Hu W, Dodelson S. 2002. *Annu. Rev. Astron. Astrophys.* 40:171
Hubble EE. 1925. *Ap. J.* 62:409
Hubble EP. 1926. *Ap. J.* 63:236
Hubble EP. 1929a. *Proc. Natl. Acad. Sci. USA* 15:168
Hubble EP. 1929b. *Ap. J.* 69:103
Huchra JP. 1992. *Science* 256:321
Humphreys EML, Reid MJ, Greenhill LJ, Moran JM, Argon AL. 2008. *Ap. J.* 672:800
Iben I, Renzini A. 1983. *Annu. Rev. Astron. Astrophys.* 21:271
Jackson N. 2007. *Living Rev. Relativ.* 10:4
Jacoby GH, Branch D, Ciardullo R, Davies RL, Harris WE, et al. 1992. *Publ. Astron. Soc. Pac.* 104:599
Jha S, Kirshner RP, Challis P, Garnavich PM, Matheson T, et al. 2006. *Astron. J.* 131:527
Jones WC, Ade PAR, Bock JJ, Bond JR, Borrill L, et al. 2006. *Ap. J.* 647:823
Kennicutt RC, Stetson PB, Saha A, Kelson D, Rawson D, et al. 1998. *Ap. J.* 498:181
Kolb EW, Turner MS. 1990. *The Early Universe*. Redwood City, CA: Addison-Wesley
Komatsu E, Dunkley J, Nolta MR, Bennett CL, Gold B, et al. 2009. *Ap. J. Suppl.* 180:330

Komatsu E, Smith KM, Dunkley J, Bennett CL, Gold B, et al. 2010. *Ap. J. Suppl.* Submitted (arXiv 1001.4538)
Kowal CT. 1968. *Astron. J.* 73:1021
Krauss LM, Chaboyer B. 2003. *Science.* 299:65
Leavitt HS. 1908. *Ann. Harv. Coll. Obs.* 60:87
Leavitt HS, Pickering EC. 1912. *Harv. Coll. Obs. Circulars* 173:1
Lee MG, Freedman WL, Madore BF. 1993. *Ap. J.* 417:553
Lemaître G. 1927. *Ann. Soc. Sci. Brux.* 47:49
Lo KY. 2005. *Annu. Rev. Astron. Astrophys.* 43:625
Macri LM, Stanek KZ, Bersier D, Greenhill LJ, Reid MJ. 2006. *Ap. J.* 652:1133
Madore BF. 1982. *Ap. J.* 253:575
Madore BF, Freedman WL. 1991. *PASP* 103:933
Madore BF, Freedman WL. 2005. *Ap. J.* 630:1054
Madore BF, Freedman WL. 2009. *Ap. J.* 696:1498
Madore BF, Freedman WF, Rigby J, Persson SE, Sturch L, Mager V. 2009. *Ap. J.* 695:988
Madore BF, Mager V, Freedman WF. 2009. *Ap. J.* 690:389
Mager V, Madore BF, Freedman WF. 2008. *Ap. J.* 689:721
Maoz E, Newman JA, Ferrarese L, Stetson PB, Zepf SE, et al. 1999. *Nature* 401:351
McGaugh SS, Schombert JM, Bothun GD, de Blok WJG. 2000. *Ap. J. Lett.* 533:L99
Moehler S, Bono G. 2008. In *White Dwarfs*, ed. M Burleigh, R Napiwotzki. Springer Verlag, ASSL. In press
Mould J, Sakai S. 2008. *Ap. J. Lett.* 686:L75
Mould J, Sakai S. 2009a. *Ap. J.* 694:1331
Mould J, Sakai S. 2009b. *Ap. J.* 697:996
Mould JR, Huchra JP, Freedman WL, Kennicutt RC, Ferrarese L, et al. 2000. *Ap. J.* 529:786
Myers ST. 1999. *Proc. Natl. Acad. Sci. USA* 96:4236
Newman JA, Ferrarese L, Stetson PB, Maoz E, Zepf SE, et al. 2001. *Ap. J.* 553:562
Ngeow C, Kanbur SM, Nanthakumar A. 2008. *Astron. Astrophys.* 477:621
Nolta M, Dunkley J, Hill RS, Hinshaw G, Komatsu E, et al. 2009. *Ap. J. Suppl.* 180:296
Peebles PJE, Yu JT. 1970. *Ap. J.* 162:815
Percival WJ, Reid BA, Eisenstein DJ, Bahcall NA, Budavari T, et al. 2009. *MNRAS* 401:2148
Perlmutter S, Aldering G, Goldhaber G, Knop RA, Nugent P, et al. 1999. *Ap. J.* 517:565
Phillips MM. 1993. *Ap. J. Lett.* 413:L105
Pierce MJ, Tully RB. 1988. *Ap. J.* 330:579
Pskovskii YP. 1984. *Sov. Astron.* 28:658
Readhead ACS, Mason BS, Contaldi CR, Pearson TJ, Bond JR, et al. 2004. *Ap. J.* 609:498
Refsdal S. 1964. *MNRAS* 128:307
Reichardt C, Ade PAR, Bock JJ, Bond JR, Brevik JA, et al. 2009. *Ap. J.* 694:1200
Reid MJ, Braatz JA, Condon JJ, Greenhill LJ, Henkel C, et al. 2009. *Ap. J.* 695:287
Riess AG, Filippenko AV, Challis P, Clocchiatti A, Diercks A, et al. 1998, *Ap. J.* 116:1009
Riess AG, Macri L, Casertano S, Sosey M, Lampeitl H, et al. 2009a. *Ap. J.* 699:539
Riess AG, Macri L, Li W, Lampeitl H, Casertano S, et al. 2009b. *Ap. J. Suppl.* 183:109
Rizzi L, Tully RB, Makarov D, Makarova L, Dolphin AE, et al. 2007. *Ap. J.* 661:81
Romaniello M, Primas F, Mottini M, Pedicelli S, Lemasle B, et al. 2008. *Astron. Astrophys.* 488:731
Romaniello M, Primas F, Mottini M, Pedicelli S, Lemasle B, et al. 2010. *Stellar Pulsation: Challenges for Theory and Observation*, ed. J Guzik, P Bradley. *AIP Conf. Proc.* 1170:99
Rowan-Robinson M. 1985. *The Cosmological Distance Ladder: Distance and Time in the Universe*. New York: Freeman
Saha A, Sandage AR, Tammann GA, Labhardt L, Macchetto FD, et al. 1999. *Ap. J.* 522:802
Sakai S, Ferrarese L, Kennicutt RC, Saha A. 2004. *Ap. J.* 608:42
Sakai S, Mould JR, Hughes SMG, Huchra JP, Macri LM, et al. 2000. *Ap. J.* 529:698
Sandage AR. 1958. *Ap. J.* 127:513
Sandage AR, Bell RA, Tripicco MJ. 1999. *Ap. J.* 522:250
Sandage AR, Gratton L. 1963. In *Star Evolution*, p. 11. New York: Academic
Sandage AR, Saha A, Tammann GA, Labhardt L, Panagia N, et al. 1990. *Ap. J. Lett.* 460:L15

Sandage AR, Tammann GA. 1968. *Ap. J.* 151:531
Sandage AR, Tammann GA. 1982. *Ap. J.* 265:339
Sandage AR, Tammann GA. 1990. *Ap. J.* 365:1
Sandage AR, Tammann GA. 2006. *Annu. Rev. Astron. Astrophys.* 44:93
Schechter PS. 2005. In *Gravitational Lensing Impact on Cosmology*, Vol. 225, ed. Y Mellier, G Meylan, p. 281. Cambridge, UK: Cambridge Univ. Press
Scowcroft V, Bersier D, Mould JR, Wood PR. 2009. *MNRAS* 396:1287
Shapley H. 1930. *Star Clusters*. New York: McGraw-Hill
Sneden C, Cowan JJ, Beers TC, Truran JW, Lawler JE, et al. 2001. *Astrophys. Ages Times Scales* 245:235
Soszynski I, Poleski R, Udalski A, Szymanski MK, Kubiak M, et al. 2008. *Acta. Astron.* 58:163
Spergel DN, Verde L, Peiris HV, Komatsu E, Nolta MR. 2003. *Ap. J. Suppl.* 148:175
Steinmetz M, Navarro J. 1999. *Ap. J.* 513:555
Sunyaev R, Zel'dovich Y. 1969. *Astrophys. Space Sci.* 4:301
Sunyaev R, Zel'dovich Y. 1970. *Astrophys. Space Sci.* 7:3
Suyu SH, Marshall PJ, Auger MW, Hilbert S, Blandford RD, et al. 2009. *Ap. J.* 691:277
Tammann GA, Sandage AR, Reindl B. 2008. *Astron. Astrophys. Rev.* 15:289
Tonry JL, Blakeslee JP, Ajhar EA, Dressler A. 2002 *Ap. J.* 530:625
Tonry JL, Schneider DP. 1988. *Ap. J.* 96:807
Tully RB, Fisher JR. 1977. *Astron. Astrophys.* 54:661
Tully RB, Pierce MJ. 2000. *Ap. J.* 553:744
Udalski A, Wyrzykowski L, Pietrzynski G, Szewczyk O, Szymanski M, et al. 2001. *Acta. Astron.* 51:221
van den Bergh S. 1992. *Publ. Astron. Soc. Pac.* 104:861
Whelan J, Iben IJ. 1973. *Ap. J.* 186:100
Wood-Vasey WM, Friedman AS, Bloom JS, Hicken M, Modjaz M, et al. 2008. *Ap. J* 689:377

Annual Review of Astronomy and Astrophysics

Volume 48, 2010

Contents

Indexes

Errata

An online log of corrections to *Annual Review of Astronomy and Astrophysics* articles may be found at http://astro.annualreviews.org/errata.shtml